Title

Relative contributions and mapping of ventral tegmental area dopamine and GABA neurons by projection target in the rat

Journal

The Journal of Comparative Neurology, 527(5)

ISSN

1550-7149

Authors

Breton, Jocelyn M
Charbit, Annabelle R
Snyder, Benjamin J
et al.

Publication Date

2019-04-01

DOI

10.1002/cne.24572

Peer reviewed

Published in final edited form as:

J Comp Neurol. 2019 April 01; 527(5): 916–941. doi:10.1002/cne.24572.

Relative Contributions and Mapping of Ventral Tegmental Area Dopamine and GABA Neurons by Projection Target in the Rat

Jocelyn M. Breton[1], **Annabelle R Charbit**[2], **Benjamin J. Snyder**[2], **Peter T.K. Fong**[2,3], **Elayne V. Dias**[3], **Patricia Himmels**[3], **Hagar Lock**[3], and **Elyssa B. Margolis**[2,3]

[1]Helen Wills Neuroscience Institute, University of California, Berkeley, Berkeley, California 94720

[2]Department of Neurology and Wheeler Center for the Neurobiology of Addiction, University of California, San Francisco, California 94143

[3]Ernest Gallo Clinic and Research Center, University of California, San Francisco, Emeryville, California 94608

Abstract

The ventral tegmental area (VTA) is a heterogeneous midbrain structure that contains dopamine (DA), GABA and glutamate neurons that project to many different brain regions. Here we combined retrograde tracing with immunocytochemistry against tyrosine hydroxylase (TH) or glutamate decarboxylase (GAD) to systematically compare the proportion of dopaminergic and GABAergic VTA projections to ten target nuclei; anterior cingulate, prelimbic, and infralimbic cortex; nucleus accumbens core, medial shell, and lateral shell; anterior and posterior basolateral amygdala; ventral pallidum; and periaqueductal gray. Overall, the *non*-dopaminergic component predominated VTA efferents, accounting for more than 50% of all projecting neurons to each region except the nucleus accumbens core. Additionally, GABA neurons contributed no more than 20% to each projection, with the exception of the projection to the ventrolateral periaqueductal gray, where the GABAergic contribution approached 50%. Therefore, there is likely a significant glutamatergic component to many of the VTA's projections. We also found that VTA cell bodies retrogradely labeled from the various target brain regions had distinct distribution patterns within the VTA, including in the locations of DA and GABA neurons. Despite this patterned organization, VTA neurons comprising these different projections were intermingled and never limited to any one sub-region. These anatomical results are consistent with the idea that VTA neurons participate in multiple distinct, parallel circuits that differentially contribute to motivation and reward. While attention has largely focused on VTA DA neurons, a better understanding of VTA sub-populations, especially the contribution of non-DA neurons to projections, will be critical for future work.

Graphical Abstract

Current Addresses:

Peter Fong's present address is: Touro University California, College of Osteopathic Medicine, Vallejo, California 94592; Patricia Himmels's present address is: Genentech Inc. 1 DNA Way, South San Francisco, California 94080; Elayne Dias's present address is: Department of Structural and Functional Biology, Institute of Biology, University of Campinas, Campinas, SP, Brazil 13083-865; and Hagar Lock's present address is: Calle Alonso Cano 11D, Bellaterra, Barcelona, Spain, 08193

We combined retrograde tracing with immunocytochemistry to compare the proportion of dopaminergic and GABAergic ventral tegmental area (VTA) neurons by projection, and characterized their topographical distribution within the VTA. In almost all cases, dopaminergic projections made up less than 50% of the overall projection to each target nuclei.

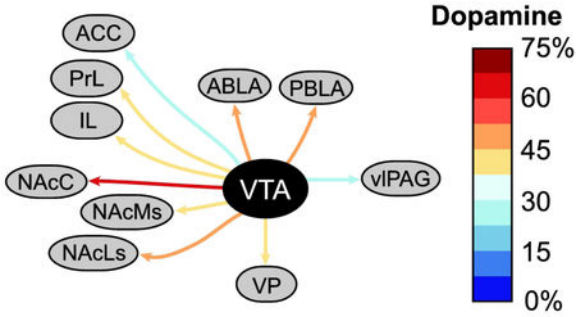

Keywords

ventral tegmental area; dopamine; GABA; retrograde; immunocytochemistry; RRID: AB_390204; RRID: AB_2278725; RRID: SCR_003070

INTRODUCTION

The VTA is critically involved in the neural processes that underlie motivation and reward (Fields, Hjelmstad, Margolis, & Nicola, 2007; Morales & Margolis, 2017; Wise & Rompre, 1989). For example, stimulation of VTA dopamine (DA) neurons can produce positive reinforcement and conditioned place preference (Adamantidis et al., 2011; Ilango et al., 2014; Steinberg et al., 2014; Tsai et al., 2009). In addition, blocking glutamatergic drive onto VTA neurons is sufficient to prevent the rewarding effects of systemically administrated drugs of abuse such as morphine and cocaine (Harris & Aston-Jones, 2003; Harris, Wimmer, Byrne, & Aston-Jones, 2004). Both these lines of evidence indicate that the firing of VTA neurons produces positive reinforcement.

However, while the VTA is thought of as a primarily dopaminergic region, almost half of its constituent neurons are *not* dopaminergic (Margolis, Lock, Hjelmstad, & Fields, 2006; Root et al., 2016; Swanson, 1982; Yamaguchi, Wang, Li, Ng, & Morales, 2011) and DA neurons are actually in the minority in most VTA projections (Swanson, 1982). While there is evidence for local GABAergic connections (Johnson & North, 1992; Omelchenko & Sesack, 2009; Van Zessen, Phillips, Budygin, & Stuber, 2012), GABA, as well as glutamate, VTA projection neurons are clearly more common than initially hypothesized, and these neurons are sufficient to drive behavior independently from DA (Carr & Sesack, 2000; Gorelova, Mulholland, Chandler, & Seamans, 2012; Yamaguchi et al., 2011; for a review see Morales & Margolis, 2017). For instance, VTA GABA neurons fire in response to aversive stimuli and cues predicting a subsequent reward (Cohen, Haesler, Vong, Lowell, & Uchida, 2012; Tan et al., 2012). The fact that DA neurons fire in response to the same reward predicting cues is inconsistent with cue responsive GABA neurons being local interneurons, raising the possibility that they are actually projection neurons. Furthermore, stimulating GABA

projections from the VTA to the nucleus accumbens (NAc) enhances associative learning (Brown et al., 2012). The sheer number of non-DA VTA projection neurons and the prima facie evidence for their role in behavior independent of DA neurons, calls for more careful characterization of these subpopulations.

Rather than being a homogeneous population, the VTA contains multiple sub-regions: the parabrachial pigmented area (PBP), paranigral nucleus (PN), and the midline interfascicular nucleus, and rostral and caudal linear nuclei. Distinct subsets of VTA neurons also project to different target structures, with little axon collateralization (Lammel, Lim, & Malenka, 2014; Margolis, Lock, Hjelmstad, et al., 2006; Swanson, 1982). For example, there are diverse VTA projections to the anterior cingulate cortex (ACC), medial prefrontal cortex (mPFC), nucleus accumbens (NAc), ventral pallidum (VP), basolateral amygdala (BLA), and ventrolateral periaqueductal gray (vlPAG) (Carr & Sesack, 2000; Fallon, Schmued, Wang, Miller, & Banales, 1984; Fields et al., 2007; Margolis, Lock, Chefer, et al., 2006; Pierce & Kumaresan, 2006; Swanson, 1982). Although tracing studies have been done for many of these projections individually, here we have examined the projections to each of these nuclei in parallel, and quantified not only DA but also GABA contributions. A number of prior studies describe the distribution of axon fibers within target nuclei, which does not provide information about the distribution of cell bodies within the VTA (Beckstead, Domesick, & Nauta, 1979; Kirouac & Pittman, 2000). This information is important because there is evidence that there are differences in behavioral contributions of the VTA along the anterior-posterior (AP) and medial-lateral (ML) axes (Beier et al., 2015; Ikemoto, 2007; Lammel et al., 2012; Taylor et al., 2014; reviewed in Barrot 2014).

Here we systematically investigated two aspects of the topography of VTA projection neurons. First, we quantified the distribution of the cell bodies within the VTA that contribute to each investigated projection. Second, we determined the proportion of those neurons that expressed either tyrosine hydroxylase (TH), the rate-limiting enzyme of DA production, or the 67 kDa isoform of glutamate decarboxylase (GAD), the enzyme that converts glutamate to GABA. We defined the VTA as the entire region overlapping with the A10 cell group, and to facilitate comparisons to AP and ML behavioral differences, we specifically examined projections in three distinct VTA regions of interest in horizontal brain slices: posterior lateral, anterior lateral and medial VTA, at multiple dorsal ventral (DV) levels. Consistent with prior reports, the neurons comprising different projections are concentrated in particular sub-regions of the VTA, yet even within these sub-regions, the proportions of dopaminergic and GABAergic neurons contributing to each projection varied widely. Interestingly, we also found novel differences in the VTA projections to adjacent target regions that have not been discriminated in prior studies, such as the anterior and posterior BLA, and between sub-regions of the mPFC. Together, these data show distinct patterns of projection neuron distributions and their phenotypes arising from the VTA.

MATERIALS AND METHODS

All experimental procedures conformed to National Institutes of Health, UCSF and Ernest Gallo Clinic and Research Center animal care policy standards, and were approved in

advance by the University of California, San Francisco and Ernest Gallo Clinic Institutional Animal Care and Use Committees.

Injection of tracer

Most experiments were completed in male Sprague Dawley rats (n = 80 Harlan), weighing 275-375g. In a small subset of experiments, younger animals weighing 80 - 100g (n = 10 Harlan) were used; we previously demonstrated physiological properties, including those that sort with projection target, of VTA neurons in rats of this age are not different from observations in adult rats. (Margolis, Mitchell, Ishikawa, Hjelmstad, & Fields, 2008). Therefore all animals were analyzed together. Rats were anesthetized with isoflurane and mounted onto a stereotaxic frame (Model 900 stereotaxic frame, David Kopf Instruments, USA). The skull was exposed and a craniotomy was performed unilaterally above the stereotaxic coordinates of one of the projection nuclei of the VTA (schematic in Figure 1a). No obvious hemispheric differences were detected, so all data for a specific nucleus were pooled. For animals undergoing protocol A (Table 1), a stainless steel 26 gauge guide cannula (C315GS-4/SPC, Plastics One Inc.) was then lowered to the chosen stereotaxic coordinates. A stainless steel 33 gauge injection cannula (C315FDS-4/SPC, Plastics One Inc.), connected by tubing to a 1 ml Hamilton syringe, was front-filled with retrograde tracer, Neuro-DiI (7% in EtOH; Biotium), and then attached to an infusion pump. The injection cannula was inserted into the guide cannula, and 0.3 μl of Neuro-DiI was injected at a rate of 0.1 μl/min. For animals undergoing protocol B, a nanoliter injector (Nanoject II, Drummond Scientific Co.) was prepared with a glass capillary injector tip front-filled with Neuro-DiI. The glass injector tip was lowered to the chosen stereotaxic coordinates, and then 70-100 nl of Neuro DiI was injected at a rate of 18-20 nl/15 seconds (72-80 nl/min) (Table 1). Surgical coordinates for all tracer injections are reported in Table 2.

Perfusion and histology

At least seven days (and no more than 14 days) after the surgery, rats were deeply anesthetized with sodium pentobarbital 200 mg/kg (Euthasol®, Vibrac AH Inc.), and transcardially perfused with saline solution, followed by either 10% buffered formalin (245-684, Fisher Scientific) or fresh 4% paraformaldehyde. Brains were removed, and post-fixed for a minimum of two and maximum of four hours in either 10% formalin or 4% paraformaldehyde (protocol A or B, respectively).

Coronal brain slices (50 μm) containing the injection region were cut using a Vibratome (Leica VT1000S), with the exception of the vlPAG, where horizontal sections were cut due to proximity to the VTA. Alternating slices were stained with cresyl violet in order to better visualize brain structures, while unstained slices provided a better visualization of DiI spread. All slices containing DiI were then mounted on glass slides, cover-slipped (Vectashield H-1000, Vector Laboratories Inc.), and imaged using a stereomicroscope (Zeiss Stemi 2000-C). Injections were considered on target if the densest area of dye fell within the target brain region with little to no (less than 5%) spread into neighboring regions (Figure 1a and see panels a and b in Figures 3-12). Animals that were off target were not included in the analysis.

If the injection was on target, horizontal brain slices (50 μm) containing the VTA were cut using a Vibratome (Leica VT1000S). VTA slices spanning the dorsal to ventral extent of the VTA (approximately 7.60 mm to 8.42 mm ventral from skull surface according to Paxinos & Watson, 1998) were immunocytochemically processed for either TH or GAD (Figure 1b-e). Every second slice was processed, and among these, labeling was alternated between TH and GAD. In each animal, the initial, most ventral VTA slice was chosen by the geometry of the interpeduncular fossa (IPF) (approximately 8.60 mm to 8.42 mm ventral to bregma; Figure 1e). Slices were considered dorsal to the VTA when there were no TH(+) cell bodies detected in either of the lateral counting regions. This approach yielded approximately 4 slices per antibody treatment per animal.

Immunocytochemistry

Immunofluorescence was used to detect TH, the rate-limiting enzyme in the production of DA, or the 67 kDa isoform of GAD, the enzyme that converts glutamate into GABA. All immunocytochemical reactions were performed on free-floating sections. Antibodies were diluted in 0.1M PBS (pH 7.4). Sections were incubated for 2 hr in 5% normal goat serum (5% in 0.1 M PBS; S-1000, Vector Laboratories Inc.), then incubated overnight at 4°C in either rabbit anti-TH 1:200 (EMD Millipore Cat# AB152, RRID: AB_390204) or mouse anti-GAD67, clone 1G10.2 1:200 (EMD Millipore Cat# MAB5406, RRID: AB_2278725) (Table 3a). For a subset of sections, tissue was maintained in primary antibody at room temperature for the first two hours of the anti-GAD67 incubation. Following rinses in PBS (6 × 10 min), sections were incubated for two hours in secondary antibody (Table 3b), either Fluorescein (FITC)-conjugated goat antirabbit 1:500 (111-095-03, Jackson ImmunoResearch Labs Inc.), or biotinylated goat anti-mouse 1:500 (BA-9200, Vector Laboratories), followed by FITC-conjugated Avidin D (SP-2040, Vector Laboratories). Sections were then rinsed in PBS (6 × 10 min), mounted on glass slides, and cover-slipped (Vectashield H-1000, Vector Laboratories Inc.).

Antibody characterization

We have used this polyclonal rabbit anti-TH antibody to immunolabel DA neurons in the VTA previously (Berthet et al., 2014; Hjelmstad, Xia, Margolis, & Fields, 2013; Margolis, Coker, Driscoll, Lemaître, & Fields, 2010; Margolis, Toy, Himmels, Morales, & Fields, 2012). It has also been characterized in the VTA of zebra finches (Gale, Person, & Perkel, 2008). This antibody detects a single band of 62 kDa on Western blots in most species, which corresponds to TH (manufacturer's technical information). The immunolabeling pattern of this antibody within the VTA here (Figure 1d and e) was very similar to that in another study in which VTA DA neurons in the Wistar rat were immunolabeled with the same antibody (Yang et al., 2009). This antibody appears in the Journal of Comparative Neurology Antibody Database.

We have used this monoclonal mouse anti-GAD67 antibody to immunolabel GABA neurons in the VTA in prior studies (Margolis, Lock, Chefer, et al., 2006; Margolis et al., 2012; Margolis, Lock, Hjelmstad, et al., 2006). This mouse antibody against GAD has been shown to react with the 67 kDa isoform of GAD from rat, mouse, and human (manufacturer's technical information). It displayed no detectable cross reactivity with the 65 kDa isoform of

GAD on Western blots of rat brain lysate compared to antibody AB1511 (Chemicon) that reacts with bGAD65 and GAD67 (Biancardi, Campos, & Stern, 2010). This antibody appears in the Journal of Comparative Neurology Antibody Database.

Microscopic imaging and cell counting

Immunostained sections were examined and images for analysis were obtained using a confocal microscope (Zeiss LSM510 META; LSM Image Browser, Zeiss) or a widefield fluorescence microscope (Zeiss Axioskop 2; Neurolucida, MBF Bioscience) (Table 1). Images for figures were obtained on a Nikon confocal microscope (Nikon Ti, Micro-Manager). Example images of horizontal slices immunocytochemically labeled for TH are provided in Figure 1e. For cell counting, we placed three sampling windows within the VTA per hemisphere and counted on both ipsilateral and contralateral sides. Specifically, one sampling window was in the anterior lateral VTA (AL), one in the posterior lateral VTA (PL), and one in the medial VTA (M) (Figure 1c and d). Each counting window was 368 × 368 μm. The medial terminal nucleus of the accessory optic tract (MT) and the IPF were used as landmarks to consistently localize counting regions across slices and animals. Specifically, the AL and PL sampling windows were placed by dividing the MT in half and placing the non-overlapping, non-adjacent sampling windows anterior and posterior to that split, within the VTA. The medial sampling window was placed adjacent to the midline at the AP level of the MT. In more ventral slices where the fossa was large and overlapped with this location, the medial window was placed just anterior to the fossa. Counting of DiI(+) cells and quantification of co-localization with TH(+) or GAD(+) was manually completed in ImageJ (NIH, https://imagej.net, RRID: SCR_003070). A subset of animals was blind counted by two or more experimenters in order to ensure that cell counting was consistent across observers.

Cells were considered DiI(+) if there was punctate labeling in the red channel distributed throughout the soma and very proximal dendrites that was higher than background fluorescence, sufficient to readily detect neuronal shape, and if this pattern was absent in the FITC fluorescent channel. To estimate the contribution of each counting window to the overall projection, the percentage of DiI was calculated as the number of DiI(+) cells in that window divided by the total number of DiI(+) cells for that animal. To determine the percentage of VTA DA or GABA neurons that project to a specific brain region, we counted the number of DiI(+) neurons within each sampling window, and determined the proportion of those cells that were co-labeled for either TH or GAD. Co-labeling data are presented as overall percent for each target region in Figure 2 (e.g. (Total DiI(+)&TH(+))/(Total DiI(+))) as well as percent co-labeled within a given window (e.g. Figure 3e and Figure 3g). All results are presented as mean ± S.E.M.

RESULTS

We labeled VTA projections with the retrograde transport of the tracer DiI, a lipophilic label that is passively incorporated into the plasma membrane of cells, and then quantified the distribution of labeled neurons within the VTA. Furthermore, we quantified the co-localization of immunocytochemical labeling for TH or GAD in DiI(+) neurons as markers

for DA and GABA neurons, respectively. We investigated VTA projections to anterior cingulate cortex (ACC), prelimbic cortex (PrL), infralimbic cortex (IL), nucleus accumbens core (NAcC), nucleus accumbens medial shell (NAcMs), nucleus accumbens lateral shell (NAcLs), ventral pallidum (VP), anterior basolateral amygdala (ABLA), posterior basolateral amygdala (PBLA), and the ventrolateral periaqueductal gray (vlPAG) (Figure 1a, Table 2). We completed analysis of 3-12 animals per projection (average five animals). All injections were unilateral into either the left or right hemisphere; data were grouped together as we observed no hemispheric differences. We counted labeled neurons within six sampling windows (three ipsilateral, three contralateral) in each analyzed horizontal slice through the dorsal-ventral (DV) axis of the VTA (Figure 1d). We made horizontal sections as they facilitate direct comparison of medial, anterior lateral and posterior lateral regions. While raw cell counts are highly dependent upon injection volume, tracer diffusion, and anatomy of injection site, the highest overall cell counts were seen in VTA projections to the VP (110 ± 14 cells ipsi, 20 ± 9 cells contra) and ACC (99 ± 19 ipsi, 50 ± 5 contra, on average). The projections from the VTA to the NAc sub-regions and to the vlPAG also had the next highest counts, with 60-75 cells in the ipsilateral projection, on average (NAcC: 67 ± 8 cells ipsi, 7 ± 3 cells contra; NAcMs: 75 ± 18 cells ipsi, 16 ± 7 cells contra; NAcLs: 60 ± 16 cells ipsi, 2 ± 1 cells contra; vlPAG: 66 ± 18 cells ipsi, 49 ± 14 cells contra). In contrast, the sparsest overall counts were in VTA projections to the PrL (31 ± 5 ipsi, 6 ± 1 contra) and IL (26 ± 4 ipsi, 3 ± 1 contra). Cell counts to the ABLA and PBLA fell in the middle of the range (ABLA: 46 ± 8 cells ipsi, 7 ± 3 cells contra; PBLA: 55 ± 5 cells ipsi, 14 ± 2 cells contra). Sparser projections, especially contralateral projections, produced some variability in the quantification of TH and GAD co-localization in some cases.

Cortical projections

The medial walls of the rodent frontal cortex are involved in emotional and reward related behaviors (Etkin, Egner, & Kalisch, 2011; Tzschentke, 2000). This region consists of the anterior cingulate cortex and the medial prefrontal cortex (mPFC). Previous studies of VTA projections have not differentiated PrL and IL within the mPFC (Carr & Sesack, 2000; Chandler, Lamperski, & Waterhouse, 2013; Deutch et al., 1991; James H. Fallon et al., 1984; Seroogy, Dangaran, Lim, Haycock, & Fallon, 1989), but since the PrL and IL have different projection targets and are implicated in different aspects of fear expression and drug seeking behavior (Gourley & Taylor, 2016; Moorman, James, McGlinchey, & Aston-Jones, 2015; Peters, LaLumiere, & Kalivas, 2008; Vidal-Gonzalez, Vidal-Gonzalez, Rauch, & Quirk, 2006), we investigated differences between them here.

Anterior cingulate cortex

Ipsilateral projections from the VTA to the ACC were modestly denser than contralateral projections: 68 ± 2% of DiI labeled VTA cell bodies were ipsilateral to the injection site (Figure 2a, Figure 3c). DiI(+) cells were relatively evenly distributed across counting windows within the ipsilateral or contralateral sides (Figure 3c). For both ipsilateral and contralateral connections, 23 ± 4% of ACC-projecting VTA neurons were co-localized with TH labeling (Figure 2c,e); the highest percentages of DiI(+)-TH(+) neurons were localized in the dorsal lateral regions (Figure 3d,e). Among contralateral projections, ACC-projecting neurons in the posterior-lateral VTA had a greater percentage of TH co-labeling (32 ± 4%)

with lower colabeling rates in the anterior-lateral and medial regions (13 ± 5% and 10 ± 2% respectively) (Figure 3e). Interestingly, many of the contralateral ACC-projecting VTA neurons were colocalized with GAD (41 ± 15%) compared to the ipsilateral projection (22 ± 6%) (Figure 2c,e). For both ipsilateral and contralateral ACC-projecting VTA neurons, the DiI co-localization with GAD was markedly enriched in the more dorsal slices compared to ventral slices, where little co-localization was detected (Figure 3f,g).

Prelimbic cortex

In contrast to ACC-projecting VTA neurons, projections from the VTA to the PrL were largely ipsilateral (82 ± 3%, Figure 2a, Figure 4c). Throughout the DV extent of the VTA, more DiI labeled cell bodies were located in midline regions, both ipsilateral and contralateral to the injection site. Looking at the distribution along the DV axis, a greater number of PrL-projecting neurons were located in the ventral VTA (Figure 4c). A similar percentage of ipsilateral and contralateral PrL-projecting neurons were co-localized with TH (38 ± 6% ipsi and 39 ± 13% contra) (Figure 2c,d,e). Not only were PrL-projecting neurons most numerous in midline structures, co-localization with TH was also highest here, especially at the mid-dorsal level. In fact, on the contralateral side, the only PrL-projecting TH(+) neurons detected were along the midline (Figure 4e). Overall, a much lower percentage of PrL-projecting cells were co-localized with GAD (12 ± 5% ipsi and 19 ± 10% contra) compared to ACC-projecting VTA neurons (Figure 2c,e,f). The percentage of GAD(+) PrL-projecting neurons was slightly higher in midline VTA regions, especially in the contralateral ventral VTA (Figure 4g).

Infralimbic cortex

Projections from the VTA to the IL were mostly unilateral, with 89 ± 3% of DiI labeled cells located ipsilateral to the injection site (Figure 2a, Figure 5c). The densest grouping of DiI(+) neurons was the medial VTA. In contrast to the PrL projection, a greater percentage of IL-projecting neurons were located in the more dorsal VTA compared to the ventral VTA (Figure 4c, 5c). A similar percentage of ipsilateral and contralateral IL-projecting cells were co-localized with TH (40 ± 7% ipsi, 37 ± 17% contra) (Figure 2c,d,e). Interestingly, the percentage of ipsilateral IL-projecting TH(+) neurons was highest in posterior lateral regions (62 ± 6%), distributed fairly evenly across the DV axis. On the contralateral side, TH(+) IL-projecting cells were located exclusively in the medial VTA, but evenly distributed across the DV slices. (Figure 5e). Only seven percent of all IL-projecting neurons were co-localized with GAD (Figure 2c,e,f). There was a uniquely high proportion of ipsilateral GAD(+) IL-projecting neurons in the posterior lateral VTA, in the mid-ventral slice, where little to no co-localization was detected in any other sampling region (Figure 5g).

Nucleus Accumbens

Within the NAc, the core and shell are neuroanatomically distinct regions (Deutch & Cameron, 1992; Zahm, 1998) that play different roles in motivated and reward related behavior (Bassareo, Cucca, Frau, & Di Chiara, 2015; Floresco, Montes, Tse, & van Holstein, 2018; Ito, Robbins, & Everitt, 2004). In addition, differences have previously been found in the mouse with respect to the distribution of VTA projections to the medial and lateral NAc shell, with medial VTA neurons projecting preferentially to the medial shell and lateral VTA

neurons projecting to lateral shell (Lammel et al., 2008). These sub-regions of the NAc shell may also play distinct roles in reward related behavior and hedonic impact (Lammel et al., 2012; Pecina & Berridge, 2005). Thus, we examined VTA projections to each region separately.

No staining for GAD was done for projections to the NAc sub-regions, as based on prior work in our lab and others, we expect the majority of the non-DA neurons to be GABAergic (Margolis, Lock, Chefer, et al., 2006; Van Bockstaele & Pickel, 1995; Yamaguchi et al., 2011). When we previously quantified TH and GAD contributions to the NAc projection with a similar counting approach for larger injections that included the NAc medial shell and core, the sum of TH(+) (66 ± 10%) and GAD(+) (25 ± 5%) neurons accounted for the vast majority of the total projection (Margolis, Lock, Chefer, et al., 2006). There is a sparse glutamatergic projection that likely accounts for that remaining <10%, and arises mostly from the medial VTA (Yamaguchi et al., 2011). Thus, in the current study, we infer that most non-DA neurons are GABAergic in the lateral VTA, where non-DA neurons in the medial VTA may be either GABAergic or glutamatergic.

Nucleus Accumbens Core

Projections from the VTA to the NAcC were highly unilateral, with 92 ± 3% of DiI labeled cells located ipsilateral to the injection site (Figure 2b, Figure 6c). The highest density of this projection was located in the lateral regions of the middle slices along the DV axis (Figure 6c). NAcC-projecting cells showed the highest percentage of co-localization with TH of any brain region in this study (64 ± 12% ipsi, 67 ± 21% contra) (Figure 2d,f). In the ipsilateral VTA, high percentages of TH(+) projection neurons were observed across many of the sampling windows and DV slices, except in the ventral medial VTA. On the contralateral side, TH(+) NAcC-projecting cells appear slightly enriched in medial regions (66 ± 6%) across the DV axis, while among lateral sampling regions a TH(+) contribution was only observed in the dorsal half of the VTA (Figure 6d,e).

Nucleus Accumbens Medial Shell

Most retrogradely labeled NAcMs-projecting VTA neurons were located ipsilateral to the injection site (83 ± 5%) (Figure 2b, Figure 7c). The majority of this projection was located in the mid to ventral VTA, but retrogradely labeled neurons were relatively evenly distributed within sampling windows of each DV plane examined; this projection was markedly sparse in the most dorsal slice of the VTA (Figure 7c). Of note, we did not observe a large population of NAcMs projecting neurons in the ventral posterior VTA just lateral to the interpeduncular nucleus, which others have previously reported (Ikemoto, 2007; Lammel et al., 2008). Forty-two ± 18% of all ipsilateral and 30 ± 15% of all contralateral NAcMs-projecting neurons were co-localized with TH (Figure 2d,f). The percentage of ipsilateral NAcMs-projecting TH(+) cells was distributed fairly evenly across the sampling windows throughout the VTA. On the contralateral side, TH(+) NAcMs-projecting neurons were somewhat enriched in the medial VTA (28 ± 3%), similar to NAcC projections (Figure 7d,e).

Nucleus Accumbens Lateral Shell

Projections from the VTA to the NAcLs were almost entirely unilateral, with 96 ± 1% of DiI labeled cells located ipsilateral to the injection site (Figure 2b, Figure 8c). Projection neurons were most dense in the lateral VTA regions, especially in the middle slices of the DV axis (Figure 8c). Similar to findings in the NAcMs projection, approximately 49 ± 2% of all ipsilateral NAcLs-projecting VTA neurons were TH(+). In contrast, only 11 ± 11% of the small number of contralateral projections were TH(+) (Figure 2d,f). On the ipsilateral side, the highest percentage of TH(+) neurons was localized in the lateral regions in the mid-ventral VTA (Figure 8d,e).

Ventral pallidum

The VP plays a significant role in driving motivated behaviors (Hubner & Koob, 1990; Richard, Ambroggi, Janak, & Fields, 2016; Smith, Tindell, Aldridge, & Berridge, 2009). The VP is made up of unique sub-regions such as the ventromedial and dorsolateral VP; these regions were too small to differentiate via retrograde tracing approaches (Root, Melendez, Zaborszky, & Napier, 2015). While the VP is generally thought of as an output pathway of the NAc with projections back to the VTA, there is also evidence that the VP receives input from the VTA (Klitenick, Eutch, Churchill, & Kalivas, 1992).

Ipsilateral projections from the VTA to the VP were much denser than contralateral projections (81 ± 4% ipsi) (Figure 2a, Figure 9c). The density of DiI filled cells was not notably different between the three sampling windows or across the DV axis (Figure 9c). A higher proportion of ipsilateral VP-projecting VTA neurons were co-labeled with TH (39 ± 7%) compared to the contralateral projection (17 ± 5%) (Figure 2c,d,e). On the ipsilateral side, the percentage of TH(+) was slightly higher in the lateral VTA compared to medial regions throughout the DV extent. On the contralateral side, VP-projecting TH(+) neurons were also located mostly in the lateral regions. These contralateral projections arose mostly from the dorsal VTA (Figure 9e). The percentage of VP-projecting VTA neurons co-localized with GAD was twice as high on the ipsilateral compared to the contralateral side (19 ± 4% ipsi, 8 ± 4% contra) (Figure 2c,e,f). The average proportion of ipsilateral GAD(+) projection cells was similar across the sample regions within a given horizontal plane, though interestingly, higher percentages of GAD(+) cells were found in dorsal compared to ventral VTA slices. This pattern also held on the contralateral side (Figure 9g).

Basolateral Amygdala

We examined projections of the VTA to different sub-regions of the BLA, the anterior and posterior BLA (ABLA and PBLA, respectively), as these two regions may play different roles in reward related behavior and send distinct outputs to sub-regions of the mPFC and NAc (Kantak, Black, Valencia, Green-Jordan, & Eichenbaum, 2002; Kim, Pignatelli, Xu, Itohara, & Tonegawa, 2016; McLaughlin & Floresco, 2007; Wright, Beijer, & Groenewegen, 1996).

Anterior Basolateral Amygdala

Projections from the VTA to the ABLA were mostly unilateral, with 87 ± 5% of DiI labeled cells located ipsilateral to the injection site (Figure 2a, Figure 10c). The density of ipsilateral

DiI projections was greatest in the anterior-lateral VTA, especially in the middle regions of the DV axis. The small contralateral projection from the VTA to the ABLA was greatest in the medial VTA (Figure 10c). Forty-seven ± 1% of all ipsilateral and 38 ± 31% of all contralateral ABLA projecting neurons were co-localized with TH, the variability on the contralateral side being driven by the small number of neurons contributing to that projection (Figure 2c,d,e). On the ipsilateral side, the highest percentages of TH(+) neurons were observed in the lateral regions, whilst on the contralateral side, TH(+) retrogradely labeled neurons were limited to medial ventral VTA (Figure 10e). Overall, a small percentage of ABLA-projecting neurons were co-localized with GAD (9 ± 3% ipsi, 11 ± 11% contra) (Figure 2c,e,f). On the ipsilateral side, GAD(+) cells were found almost exclusively in the posterior lateral regions in ventral VTA slices. On the contralateral side, GAD(+) projection neurons were also only located in lateral regions of the VTA (Figure 10g).

Posterior Basolateral Amygdala

Projections from the VTA to the PBLA were mostly ipsilateral (81 ± 2%) (Figure 2a, Figure 11c). The highest densities of projection neurons were located in the anterior lateral regions of the VTA, while the small contralateral projection was slightly greater in the medial VTA (Figure 11c). Similar to the ABLA projections, 45 ± 4% of all ipsilateral and 30 ± 8% of all contralateral PBLA-projecting VTA neurons were co-localized with TH (Figure 2c,d,e). The percentage of ipsilateral PBLA-projecting TH(+) cells was distributed fairly evenly across the sampling windows and across the DV axis. In the contralateral VTA, the highest percentage of TH(+) neurons was located in anterior-lateral regions (Figure 11e). Interestingly, VTA neurons projecting to the PBLA had a higher percentage of GAD(+) neurons (26 ± 7% ipsi, 21 ± 7% contra) compared to projections to the ABLA (9 ± 4% ipsi, 11 ± 11% contra) (Figure 2c,e,f). These GAD(+) neurons were similarly distributed across all sample windows and across the DV axis (Figure 11g).

Ventrolateral Periaqueductal Gray

Although the vlPAG is classically thought of a region involved in the control of pain (Millan, 2002), it has reciprocal connections with the VTA (Beitz, 1982; Omelchenko & Sesack, 2010) and may be more generally involved in reward, especially in opioid mediated reward pathways (Flores, Galan-Rodriguez, Ramiro-Fuentes, & Fernandez-Espejo, 2006; Motta, Carobrez, & Canteras, 2017; Olmstead & Franklin, 1997).

Intriguingly, projections from the VTA to the vlPAG were only slightly denser on the ipsilateral than on the contralateral side (58 ± 1% ipsilateral) (Figure 2a, Figure 12c). The vlPAG had the strongest contralateral projection of all the brain regions in this study. Ipsilateral and contralateral vlPAG-projecting neurons were distributed fairly evenly across the sampling windows, and across the DV axis (Figure 12c). Interestingly, slightly more contralateral vlPAG-projecting VTA neurons were co-localized with TH (29 ± 5%) compared to the ipsilateral projection (16 ± 4%) (Figure 2c,d,e). Just as the numbers of DiI(+) cells were similar across all regions, the proportion of those projections that were co-localized with TH was also relatively evenly distributed across the VTA regions and depths within the ipsilateral and contralateral sides. (Figure 12e). Of all the brain regions we

analyzed, VTA projections to the vlPAG had the highest percentage of co-labeling with GAD, approaching 50% (48 ± 6% ipsi, 49 ± 9% contra) (Figure 2c,e,f). A similar pattern was seen in both the ipsilateral and contralateral VTA: GAD(+) projection cells were enriched in lateral and absent in medial VTA in the most ventral slices, but more evenly distributed in the rest of the DV extent of the VTA (Figure 12g).

DISCUSSION

Here we systematically investigated the anatomical contributions and distributions of DA and GABA neurons within the VTA that project to ten different target nuclei. We described the location of these projection neurons within the different sub-regions of the VTA, adding more resolution than previously provided. Additionally, we described VTA projections to regions that have not been investigated separately in prior studies, such as to the anterior and posterior BLA. We found that these efferent projections of the VTA varied not only in their somatic locations within the VTA but also in their dopaminergic and GABAergic content. Looking broadly at the differences between projections to all of the target regions, we observed an unusually high rate of contralateral VTA projections to the vlPAG and ACC, while the NAcC and NAcLs had almost exclusively ipsilateral contributions (Figure 2a,b). We observed the greatest proportion of TH(+) neurons within the projection to the NAcC (Figure 2d,f) and the greatest proportion of GAD(+) neurons within the projections to the vlPAG and to the contralateral ACC (Figure 2c,e). The projection containing the smallest percentage of TH(+) somata was to the vlPAG while the smallest percentages of GAD(+) somata were observed in the ABLA and IL projections (Figure 2c,e). While distribution patterns were distinct between projections, each target region received inputs from neurons within every ipsilateral sampling region, indicating that intermingled VTA neurons can project to different targets. Also, sub-regions of the same target structure (i.e. ABLA vs. PBLA) and adjacent structures (i.e. PFC areas) receive inputs from different parts of the VTA with different neurotransmitter content. Together, our findings reveal a patterned but intermixed organization of the VTA.

Technical considerations

Several methodological points should be considered in the interpretation of our results. First, the very dorsal portions of the linear nuclei were not represented in our data due to the geometry of the VTA in the horizontal plane. This includes a small population of ventral, posterior VTA neurons as well as a dorsal, posterior group of DA neurons located right along the midline (Figure 1e). Overall however, this represents a minor proportion of all VTA/A10 neurons. Horizontal sections provided a better layout of the VTA for comparing projections across the ML and AP axes, which have been compared in a variety of behavioral studies (reviewed in Sanchez-Catalan, Kaufling, Georges, Veinante, & Barrot, 2014 and Lammel et al., 2014, and see below). Horizontal slices of the VTA are also commonly used for *ex vivo* electrophysiology experiments, as many efferent and afferent projections of the VTA remain more intact when sectioned along the horizontal plane (Calabresi, Lacey, & North, 1989; Williams, North, Shefner, Nishi, & Egan, 1984). In the current study, a horizontal layout is not only informative for our anatomical analysis, but also allows us to more directly compare our results with VTA electrophysiology work.

Another technical issue inherent in any experiment that relies on microinjection of a reagent is incomplete coverage of the target nucleus. In the present study, DiI injections were always smaller than the entire brain region of interest in order to prevent spread to neighboring regions. However, a small amount of dye would occasionally spread to an adjacent region; this was observed in several NAcMs injections that spread into the NAcC. Additionally, shapes of brain regions are often irregular (such as the VP). For both of these reasons, some portions of the projections may not be represented in our counts. That said, smaller injections targeting different parts of certain brain regions enabled us to detect differences between VTA projections to the ABLA and PBLA, and among the projections to the NAcC, NAcMs, and NAcLs. Furthermore, we adjusted the volumes of DiI injected in order to maximize coverage of the target nucleus and minimize spread outside that target. However, since injections and tracer uptake never capture an entire projection, we chose to normalize our data and do not draw strong conclusions from differences in absolute counts between projection target groups.

Lastly, there are inherent limitations of immunocytochemistry techniques that may have impacted our results. For example, there is always the possibility that protein levels were too low to be immunocytochemically detected in a subset of neurons, and therefore our percentages may be underestimates. This is an unlikely issue for TH detection, given reports of virtually complete overlap of TH immunocytochemistry with genetic reporters in the VTA (Margolis et al., 2010; Witten et al., 2011). On the other hand, there is a small subset of VTA neurons that express TH but not the vesicular monoamine transporter (VMAT2), making these neurons capable of synthesizing DA, but not packaging it into vesicles by the expected mechanism (Li, Qi, Yamaguchi, Wang, & Morales, 2013). Therefore, it is possible that a small portion of TH(+) neurons do not synaptically release DA, as has been observed in the VTA projection to the lateral habenula (Root et al., 2014). Somatic GAD labeling is less reliable, and may contribute to an underestimate of the GABAergic component of the projections studied here. Identifying GAD co-localization is also confounded by high signal in terminals, which hinders accurate counting by obscuring the difference between signal inside and outside the retrogradely labeled neurons. Therefore, undercounting GABA neurons may account for some of the “unidentified” DiI(+) neurons reported here. On the other hand, there are also many glutamate neurons in the VTA that likely contribute to these VTA projections (Gorelova et al., 2012; Hnasko, Hjelmstad, Fields, & Edwards, 2012; Morales & Root, 2014; Yamaguchi et al., 2011). Glutamate may also be utilized as a neurotransmitter in VTA neurons that express TH or GAD, meaning that some of the TH(+) or GAD(+) neurons we identified may also be glutamatergic (Morales & Root, 2014; Root et al., 2018; Stuber, Hnasko, Britt, Edwards, & Bonci, 2010; Tecuapetla et al., 2010). There is no existing immunocytochemical target for labeling VTA glutamatergic somata, as protein markers such as vesicular glutamate transporters are generally localized to terminals. Additionally, as of yet, there is no transgenic rat model to enable reporter expression selectively in glutamate neurons in the VTA. We hypothesize that the non-TH and non-GAD DiI filled cells in our study are primarily glutamatergic. Moreover, the percentages of DiI(+) neurons that were non-DA and non-GABA are consistent with prior glutamate studies in projections to the NAc and PFC (Gorelova et al., 2012; Yamaguchi et al., 2011). As tools

become available, future work should involve a similar characterization and quantification of glutamatergic projection neurons in the VTA.

Comparison with the literature

Comparison of methodologies—A variety of approaches have been used to map projections from the VTA to its target nuclei. In addition, rat and mouse anatomy may differ. For example, Taylor et al. (2014) analyzed VTA anatomy in the mouse and used a Cre-dependent mouse line to identify GABAergic neurons rather than using immunocytochemistry. Here, we implemented a retrograde tracing methodology and primarily compare our results to other rat studies that used similar methods (Kirouac, Li, & Mabrouk, 2004; Klitenick, Eutch, Churchill, & Kalivas, 1992; Margolis, Lock, Chefer, et al., 2006; Swanson, 1982; Yamaguchi et al., 2011). Anterograde-tracing methods do not allow for cell counting, but do map the relative density of terminal fibers in VTA target regions (Beckstead et al., 1979). While we did not systematically compare the overall numbers of VTA cells projecting to each region, we do see similar density patterns as prior reports. For example, using anterograde tracing, a dense projection to the VP and a sparse projection to the mPFC were previously reported (Beckstead et al., 1979; Taylor et al., 2014). Additionally, a dense bilateral projection to the vlPAG has been reported with anterograde methods (Beitz, 1982; Kirouac & Pittman, 2000). However, Aransay and colleagues (2015), using single axon anterograde tracing, reported higher rates of sparse collateralization of some VTA neurons. These neurons innervate not only the cerebral cortex but also basal forebrain regions such as the VP and amygdala. Additionally, several VTA neurons were found to innervate forebrain structures and collateralize to brainstem structures and the hypothalamus (Aransay, Rodríguez-López, García-Amado, Clascá, & Prensa, 2015). Importantly, in studies utilizing dual retrograde tracers, collateralization has been observed in only a very small proportion of VTA neurons (Fallon 1981; Loughlin & Fallon, 1984; Margolis, Lock, Chefer, et al., 2006; Swanson, 1982). Indeed, little collateralization has even been reported for projections to neighboring cortical areas (Chandler et al., 2013). While we report here that sub-regions of the VTA contribute to inputs to various projection targets, these data cannot be used to infer collateralization of individual VTA axons. Mapping input-output relationships of VTA circuits is another approach to understanding VTA heterogeneity, and rabies mediated trans-synaptic tracing, in combination with anterograde and retrograde tracers, has been used towards this goal (Beier et al., 2015; Lammel et al., 2012). For example, Beier et al (2015) found that VTA DA neurons that project to the medial or lateral NAc receive different inputs from various brain regions. More recently, genetic approaches have been used to visualize combinations of molecular markers such as Calbindin, Otx2, and Sox6, in order to identify patterns in VTA DA projection neurons. DA neurons projecting to adjacent regions such as the NAcC and NAcMs were found to have different expressions of molecular markers, consistent with these inputs arising from different VTA DA neurons (Poulin et al., 2018). It would be interesting to see if similar molecular heterogeneity is found in GABAergic VTA projections and if comparable patterns are observed in the rat. Overall, where there is data to compare, the patterns observed with these alternate techniques are consistent with our findings, indicating that in the VTA, cell body counts using retrograde tracing corresponds well with the existing anterograde literature.

Comparison of dopaminergic projections—Where previous data exist, the proportion of DA neurons in each projection observed here is largely consistent with the literature in the rat (Kirouac et al., 2004; Klitenick et al., 1992; Margolis, Lock, Chefer, et al., 2006; Swanson, 1982; Yamaguchi et al., 2011) but was overall lower than percentages reported in the mouse (Taylor et al., 2014). For all of the subsequent comparisons, the reported percentages refer to ipsilateral projections, unless otherwise indicated. Projections to cortical regions were approximately 20-40% dopaminergic. Specifically, the projection to the ACC was around 23% TH(+), consistent with findings from Swanson (1982). A slightly higher percentage of TH(+) neurons (approx. 40%) was found in projections to the PrL and IL. This is consistent with prior reports in the rat (Margolis, Lock, Chefer, et al., 2006; Yamaguchi et al., 2011), but much less than the more than 70% DA reported in the mouse (Taylor et al., 2014). VTA projections to the NAc contained a lower percentage of DA neurons compared to several studies in the rat and mouse, which reported near 85-90% DA (Swanson, 1982; Taylor et al., 2014). However, the close to 65% TH(+) neurons observed in the projection the NAc core is consistent with prior findings in our own laboratory following injections covering the core-medial shell border (Margolis, Lock, Chefer, et al., 2006) and was greater than the reported 50% in a more recent study in the rat (Rodríguez-López, Clascá, & Prensa, 2017). The current study is the first to differentiate the percentage of DA in projections to the medial vs. lateral NAc shell in the rat. We found a similar percentage of between 40-50% TH(+) neurons in both of these projections, much less than what was reported in the mouse (Taylor et al., 2014), but similar to a study in the rat (Rodríguez-López et al., 2017). Overall, however, projections to the NAc and its sub-regions contained the highest percentages of DA neurons, consistent with overall patterns previously reported for both rats and mice (Swanson, 1982; Taylor et al., 2014; Yamaguchi et al., 2011). The percentage of TH(+) neurons in VTA projections to the VP (approx. 40%) and BLA (approx. 50%) fell within the range of prior rat work (Klitenick et al., 1992; Swanson, 1982) but again was less than that in mouse (Taylor et al., 2014). This is the first study to differentiate VTA projections specifically to the anterior and posterior BLA; a similar percentage of TH(+) projections was found in both cases. Lastly, consistent with the literature, we found that VTA the projection to the vlPAG has a significant contralateral contribution (Aransay et al., 2015; Beitz, 1982; Kirouac et al., 2004). While one study reported a lack of DA contribution to this projection (Kirouac et al., 2004), we found that a small percentage of TH(+) neurons (approximately 15% ispi, 30% contra) projects to the vlPAG, consistent with more recent work (Aransay et al., 2015).

Comparison of GABAergic projections—Few prior studies have systematically examined VTA GABA projections, especially in the rat. The relatively small contribution of GABA neurons to each projection we observed is largely consistent with prior reports in both the rat and mouse (Taylor et al., 2014; Yamaguchi et al., 2011). Although Yamaguchi and colleagues (2011) did not identify GABA directly, around 10% of projections to the mPFC were non-dopaminergic and non-glutamatergic, therefore inferred to be GABAergic. This percentage is consistent with our findings in projections to both the PrL and IL. However, we detected a higher percentage of GAD(+) neurons in the projection to the ACC, especially from the contralateral VTA (approx. 40% contra, 20% ipsi). Prior work from our lab showed that approximately 25% of projections from the VTA to the NAc are GABAergic

(Margolis, Lock, Chefer, et al., 2006). This is relatively similar to the 36% reported by others, and reports of a minimal glutamate-only projection to the NAc (Van Bockstaele & Pickel, 1995; Yamaguchi et al., 2011). Thus, we expect the majority of the non-DA neurons (approx. 40%) projecting to the NAc to be GABAergic. To our knowledge, this was the first study to quantify the contribution of GABA neurons to the VTA projections to the VP, ABLA, and PBLA in the rat. Approximately 20% of projections to the VP were GAD(+), a much greater percentage than reported in the mouse (Taylor et al., 2014). Interestingly, a greater percentage of GAD(+) neurons was found to project to the posterior BLA (~25%) compared to the anterior BLA (~10%), suggesting AP organization of VTA inputs to the amygdala. Lastly, we found a robust GABA projection from the VTA to the vlPAG: close to 50% of the projection is GAD(+), more than the previously reported 32% (Kirouac et al., 2004). Importantly, this GABA projection arose from the VTA itself; we did not include projections from the rostromedial tegmental nucleus in this study, which also provides a dense GABA projection to the lateral PAG (Aransay et al., 2015).

Topographic organization of the VTA—We found here that while topographical distributions comprising each of the investigated projections differ, it was rare for a projection to be localized exclusively to a sub-region of the VTA. Consistent with prior studies, dorsal-ventral differences were observed in the VTA projection to the mPFC (Moore & Bloom, 1978; Swanson, 1982). PrL-projecting and IL1-projecting VTA neurons were located in more ventral and more dorsal regions, respectively. This is consistent with reports that the ventral VTA projects to more dorsal target regions, while the dorsal VTA projects more ventrally (Moore & Bloom, 1978). However, we found that ACC projection neurons were distributed relatively evenly throughout the DV axis, in contrast to Swanson's finding that cingulate-projecting neurons were located preferentially in the ventral VTA (1982). This difference may be related to tracer injection location, as our ACC injections were anterior to those analyzed by Swanson (1982). Projections to the mPFC were located more robustly in the medial VTA, consistent with prior reports of a denser projection located in the midline VTA nuclei (Chandler et al., 2013; Yamaguchi et al., 2011). Interestingly, although a greater percentage of TH(+) PrL-projecting neurons were found in midline areas, consistent with prior findings (Swanson, 1982), TH(+) IL-projecting neurons were enriched in the posterior-lateral VTA. Intriguingly, we found higher percentages of GAD(+) neurons in projections to the ACC compared to the PrL and IL, especially in the dorsal VTA. These observations are also consistent with the possibility that largely non-overlapping populations of VTA neurons project to these different sub-regions of PFC. This has been demonstrated for orbital frontal cortex, mPFC, and ACC by Chandler and colleagues (2013), who used simultaneous labeling by different fluorescent retrograde tracers to analyze collateralization of VTA projections to the PFC, and detected few dual labeled neurons. Our observations suggest this lack of collateralization is also the case for even finer subdivisions of PFC, e.g. PrL and IL.

In projections to the NAc, we see a graded topographic organization, similar to what has been previously described, with medial VTA neurons projecting more to the NAcMs and lateral VTA neurons projecting more to the NAcLs (Ikemoto, 2007; Rodríguez-López et al., 2017). With single cell axon tracing techniques, dense arborization has been observed in axons targeting the NAc core or shell, with little branching to the adjacent NAc sub-regions,

consistent with these projections being largely separate (Rodríguez-López et al., 2017). There have been reports of a similar medial-lateral topographical organization for DA neurons (Ikemoto, 2007; Saunders, Richard, Margolis, & Janak, 2018); we found that the total number of projecting neurons varies in the M-L direction, but the proportions of neurons that are TH(+) projecting to the NAc and its sub-regions were relatively similar throughout the VTA, consistent with other findings (Swanson, 1982; Taylor et al., 2014; Yamaguchi et al., 2011). In projections to the VP, although the overall distribution of neurons was fairly even across the VTA, a higher percentage of TH(+) neurons was located laterally, similar to prior reports (Klitenick et al., 1992; Taylor et al., 2014). Interestingly, a novel dorsal-ventral difference was observed in GAD(+) projections to the VP, with more VP-projecting GABA neurons located in the dorsal VTA.

Dense projections to both the ABLA and PBLA were found in the lateral VTA, a very consistent finding across the literature in both rats and mice (Aransay et al., 2015; Loughlin & Fallon, 1983; Swanson, 1982; Taylor et al., 2014). More specifically, we found that ipsilateral projections arise mostly from the anterior lateral VTA, while contralateral projections arise from the medial VTA. Higher percentages of TH(+) neurons projecting to the BLA were also observed in more lateral VTA, consistent with prior findings (Swanson, 1982). Interestingly, not only was there a marked difference in the contribution of GAD(+) neurons to the ABLA and PBLA projections, there was also a difference in their topographical organization. While there was an overall lower percentage of ABLA-projecting VTA neurons that were GAD(+), we found that these comprised more of the projection from the lateral and ventral VTA; GAD(+) projections to the PBLA were more evenly distributed.

Lastly, VTA projections to the vlPAG were fairly evenly distributed throughout the VTA. Dopaminergic lateral PAG-projecting neurons have previously been reported in the PBP, which is partially overlapping with our more dorsal lateral sampling areas (Aransay et al., 2015). In addition to observing TH(+) projections in the lateral VTA, we also observed TH(+) projections to the vlPAG in the medial VTA; these projections were evenly distributed in all sampling windows and across the DV axis. The strong GABAergic projection to the vlPAG has been previously reported (Kirouac et al., 2004); we found that the GAD(+) neurons contributing to this projection were evenly distributed in the dorsal VTA, but enriched in lateral regions of the ventral VTA.

Functional implications

Projections of the VTA to target nuclei play a functional role in motivation and reward (Fields et al., 2007; Morales & Margolis, 2017). The fact that individual VTA neurons rarely collateralize to multiple projection targets (Fallon 1981; Margolis, Lock, Chefer, et al., 2006; Swanson, 1982) raises the possibility that these different projections may contribute to different aspects of behavior. A large body of research has been devoted to understanding the contribution of DA neurons to reward related behaviors (Lammel et al., 2014; Salamone & Correa, 2012; Volkow, Wise, & Baler, 2017). However, only a slight majority of VTA neurons is actually TH(+) in the rat (Kirouac et al., 2004; Klitenick et al., 1992; Margolis et al., 2006; Swanson, 1982; Yamaguchi et al., 2011), and as we show here, most VTA

projections are composed primarily of non-DA neurons. In this context, DA-independent VTA contributions to behavior are not surprising. Importantly, DA-independent VTA reward has been observed; for example, intra-VTA morphine can produce a DA-independent conditioned place preference (CPP) (Hnasko, Sotak, & Palmiter, 2005; Nader & van der Kooy, 1997). Non-DA projections have been implicated in aversion; stimulation of VTA glutamate neurons projecting to the lateral habenula or to the NAcMs is sufficient to produce aversion (Qi et al., 2016; Root et al., 2014). Clearly, further investigation of the GABAergic and glutamatergic projections of the VTA is required in order to understand their contributions to behavior.

Functional roles of VTA dopamine projections—The behavioral role of DA in many of the target regions considered here has been intensely studied. In the cortex, D1 receptor activation is implicated in effort-based decisionmaking (Rushworth, Walton, Kennerley, & Bannerman, 2004; Schweimer & Hauber, 2005; Walton, Bannerman, Alterescu, & Rushworth, 2003). DA levels in the ACC increase with either electrical stimulation of the VTA or microinjection of a mu opioid receptor agonist into the VTA (Narita et al., 2010). In behavioral studies, PrL and IL are often considered together as the “mPFC”, potentially generating inconsistent results. For instance, in one study, optogenetic stimulation of mPFC-projecting DA neurons was aversive and anxiogenic (Gunaydin et al., 2014) but in another study, *inhibition* of the mPFC-projecting DA neurons promoted susceptibility to a subsequent social defeat stressor (Chaudhury et al., 2013). Differentiating functional effects of VTA projections to the PrL and IL, rather than the mPFC as a whole, remains an interesting question, and may resolve seemingly paradoxical observations (for a review see Moorman et al., 2015). For example, injection of a DA antagonist into the PrL but not IL attenuates stress-induced reinstatement of drug seeking behavior (Capriles, Rodaros, Sorge, & Stewart, 2003).

Considerable evidence indicates that mesolimbic DA projections from the VTA to the NAc play an important role in reinforcement and in the rewarding effects of drugs of abuse (Ikemoto, 2007, 2010; Salamone, Correa, Mingote, & Weber, 2005). The NAc core and NAc shell may play unique roles in behavior. For instance, animals intra-cranially self-administer DA agonists into the NAc medial shell, but not the NAc core, indicating that the NAcMs drives reward related behaviors (Ikemoto, 2007, 2010; McBride, Murphy, & Ikemoto, 1999). Specific functional roles of VTA projections to the medial vs. lateral NAc shell are only just beginning to be parsed (Ikemoto, Quin, & Liu, 2005; Lammel et al., 2012; Pecina & Berridge, 2013; Shin, Qin, Liu, & Ikemoto, 2008).

The BLA is involved in forming associations between sensory cues and rewarding or aversive stimuli (Davis, 1992; Gallagher, 2000; LeDoux, 1996; McGaugh, 2002; Meil & See, 1997). Here, too, researchers have found a role for DA. Lesions of the VTA decrease DA content of the amygdala (James H. Fallon & Moore, 1978) and DA receptor blockage in the BLA attenuates the conditioned reinstatement of cocaine seeking behavior (Kruzich & See, 2001). More specific roles for VTA dopamine projections to the BLA remain to be explored; in particular, we do not yet know how DA projections to the anterior compared to the posterior BLA contribute to behavior.

Blockade of DA receptors in the VP reduces ethanol self-administration into the VTA (Ding, Ingraham, Rodd, & McBride, 2015). Furthermore, 6-hydroxydopamine lesions of the VP block cocaine-induced CPP (Gong, Neill, & Justice, 1996). The VP is now recognized as a reward region in its own right rather than just as a motor output nucleus (Root et al., 2015) and is thought of as an output for limbic signals, as it is receives convergent inputs from reward related brain areas including the PFC, NAc, and amygdala (Grove, 1988; Klitenick et al., 1992; Maurice, Deniau, Menetrey, Glowinski, & Thierry, 1997; Zaborszky, Gaykema, Swanson, & Cullinan, 1997). Thus, VTA projections to the VP are well situated to influence reward processing downstream of other areas.

Functional roles of VTA GABA projections—The development of genetically tagged mouse lines has relatively recently enabled the selective study of the behavioral contributions of VTA GABA and glutamate neurons that are intermixed with DA neurons. Local stimulation of VTA GABA neurons reduces reward consumption, but little is known about how the projections contribute to this behavior (Van Zessen et al., 2012). Brown and colleagues (2012) demonstrated that stimulation of NAc-projecting VTA GABA neurons inhibits cholinergic interneurons (CINs) within the NAc, and promotes stimulus-outcome learning. However, this function may still involve DA, as CINs regulate DA release in the striatum through their action on nicotinic receptors on DA axon terminals (Cachope et al., 2012; Threlfell & Cragg, 2011; Zhou, Liang, & Dani, 2001).

The function of GABA projections to many other VTA targets remains unknown; however, one interesting pattern we detected was a greater percentage of GABA projections to the PBLA compared to the projection to the ABLA. These two regions of the amygdala have recently been shown to contain different populations of neurons that have opposing effects on behavior: neurons in the ABLA respond to aversive stimuli and can disrupt reward-seeking behaviors when activated, while neurons in the PBLA respond to appetitive stimuli and are critical for reward seeking and associative conditioning (Kim et al., 2016). Stimulation of these PBLA neurons can also elicit a CPP (Kim et al., 2016). Our anatomical detection of these VTA GABA populations, as well as those that project to the ACC and vlPAG, among others, provide especially interesting future directions for investigating how the VTA contributes to motivated behavior.

Functional implications of VTA topography—The regional heterogeneity of the VTA also has important implications for behavior. Differences between the anterior and posterior VTA have been described (for a review see Sanchez-Catalan et al., 2014), and the anatomical information we provide here is consistent with this organization. For example, rats will self-administer drugs of abuse including opiates, ethanol, and nicotine into the posterior, but not the anterior, VTA (Ding et al., 2015; Ikemoto, Qin, & Liu, 2006; Zangen, Ikemoto, Zadina, & Wise, 2002). Understanding the distribution of projection neurons and their different cell types enables the formulation of predictions regarding the circuitry involved in such behaviors. For instance, we found that projections to the IL and ACC arising from the posterior-lateral VTA contain a greater percentage of TH(+) neurons. We also observed a higher percentage of GAD(+) neurons in projections to the ABLA in the posterior-lateral VTA. Different distributions of VTA cell types (DA, GABA, or glutamate)

along the AP axis, as well as differences in the target regions those cells project to, likely in concert drive the observed behavioral differences between the anterior and posterior VTA.

The medial-lateral and dorsal-ventral organization of VTA projections is also important for behavioral outcomes. For example, our current study and others suggest topographical projections from the medial-lateral VTA to medial-lateral NAc regions (Ikemoto, 2007; Lammel et al., 2008; Rodríguez-López et al., 2017; reviewed in Lammel et al., 2014). This medial-lateral distribution is behaviorally relevant, as the medial and lateral NAc shell have functionally distinct roles (Lammel et al., 2012; Pecina & Berridge, 2005). We also found that projections to the PrL and IL were located more densely in the medial VTA, and therefore may contribute to behaviors attributed to the medial VTA; yet PrL and IL projections are differentiated by their location in the DV axis. These topographical distributions within the VTA are relevant not only in regard to where to target microinjections of drugs or viruses for behavioral studies, but also with respect to the sampling of neurons for both *in vivo* and *ex vivo* electrophysiology. Overall, the heterogeneity of the VTA, both in projection target and neurotransmitter content, is an important element to be considered for understanding the functional roles of the VTA.

Conclusions

We demonstrate here that a majority of VTA projections have a majority non-dopaminergic component. We also report the distribution of the somata within the VTA that give rise to these different projections, and the proportion of those projections that are dopaminergic or GABAergic. Building on the existing literature, we found that the cell bodies contributing to these projections show unique patterns of localization within the VTA, and variation in their neurotransmitter content. Importantly, these data indicate that projections to different brain regions arise from intermingled populations of neurons across the VTA, yet adjacent projection targets likely receive inputs from different populations of VTA neurons. Together, these observations indicate an organized but intermixed structure to the VTA, including the many non-dopaminergic projection neurons therein, whose behavioral contribution is only beginning to be explored.

ACKNOWLEDGEMENTS

We would like to thank Joseph Driscoll, Vivien Lu, Ryan Young, Brian Fowler, Izumi Shimanouchi, and Catriona Miller for their technical assistance. This work was supported by the National Institutes of Health, grant numbers R01DA030529 and R01DA042025 to E.B.M.; funds were also provided by the State of California for medical research on alcohol and substance abuse through the University of California, San Francisco. Some images for this study were acquired at the Nikon Imaging Center at UCSF on equipment purchased with NIH grant 1S10OD017993-01A1.

List of Abbreviations

ABLA	Anterior basolateral amygdala
ACC	Anterior cingulate cortex
AL	Anterior-Lateral
AP	Anterior-Posterior

BLA	Basolateral amygdala
CIN	Cholinergic interneuron
Contra	Contralateral
CPP	Conditioned place preference
DA	Dopamine
DV	Dorsal-Ventral
FITC	Fluorescein
GABA	Gamma-aminobutyric acid
GAD	Glutamic Acid Decarboxylase
IL	Infralimbic cortex
IPF	Interpeduncular fossa
Ipsi	Ipsilateral
ML	Medial-Lateral
mPFC	Medial prefrontal cortex
MT	Medial terminal nucleus of the accessory optic tract
NAc	Nucleus accumbens
NAcC	Nucleus accumbens core
NAcLs	Nucleus accumbens lateral shell
NAcMs	Nucleus accumbens medial shell
PBLA	Posterior basolateral amygdala
PBP	Parabrachial pigmented area
PL	Posterior Lateral
PN	Paranigral nucleus
PrL	Prelimbic cortex
TH	Tyrosine Hydroxylase
vlPAG	Ventrolateral periaquaductal gray
VMAT2	Vesicular monoamine transporter-2
VP	Ventral pallidum
VTA	Ventral tegmental area

REFERENCES

Adamantidis AR, Tsai H-C, Boutrel B, Zhang F, Stuber GD, Budygin EA, … de Lecea L (2011). Optogenetic Interrogation of Dopaminergic Modulation of the Multiple Phases of Reward-Seeking Behavior. The Journal of Neuroscience. 10.1523/JNEUROSCI.2246-11.2011

Aransay A, Rodríguez-López C, García-Amado M, Clascá F, & Prensa L (2015). Long-range projection neurons of the mouse ventral tegmental area: a single-cell axon tracing analysis. Frontiers in Neuroanatomy, 9, 59 10.3389/fnana.2015.00059 [PubMed: 26042000]

Barrot M (2014). The ventral tegmentum and dopamine: A new wave of diversity. Neuroscience, 282, 243–247. 10.1016/j.neuroscience.2014.10.017 [PubMed: 25453764]

Bassareo V, Cucca F, Frau R, & Di Chiara G (2015). Monitoring dopamine transmission in the rat nucleus accumbens shell and core during acquisition of nose-poking for sucrose. Behavioural Brain Research, 287, 200–206. 10.1016/j.bbr.2015.03.056 [PubMed: 25827930]

Beckstead RM, Domesick VB, & Nauta WJH (1979). Efferent connections of the substantia nigra and ventral tegmental area in the rat. Brain Research, 175(2), 191–217. 10.1016/0006-8993(79)91001-1 [PubMed: 314832]

Beier KT, Steinberg EE, DeLoach KE, Xie S, Miyamichi K, Schwarz L, … Luo L (2015). Circuit Architecture of VTA Dopamine Neurons Revealed by Systematic Input-Output Mapping. Cell, 162(3), 622–634. 10.1016/j.cell.2015.07.015 [PubMed: 26232228]

Beitz AJ (1982). The organization of afferent projections to the midbrain periaqueductal gray of the rat. Neuroscience, 7(1), 133–159. 10.1016/0306-4522(82)90157-9 [PubMed: 7078723]

Berthet A, Margolis EB, Zhang J, Hsieh T, Zhang J, Hnasko TS, … Nakamura K (2014). Loss of mitochondrial fission depletes axonal mitochondria in midbrain dopamine neurons. The Journal of Neuroscience, 34(43), 14304–14317. 10.1523/JNEUROSCI.0930-14.2014 [PubMed: 25339743]

Biancardi VC, Campos RR, & Stern JE (2010). Altered balance of γ-aminobutyric acidergic and glutamatergic afferent inputs in rostral ventrolateral medulla-projecting neurons in the paraventricular nucleus of the hypothalamus of renovascular hypertensive rats. Journal of Comparative Neurology, 518(5), 567–585. 10.1002/cne.22256 [PubMed: 20034060]

Brown MTC, Tan KR, O'Connor EC, Nikonenko I, Muller D, & Luscher C (2012). Ventral tegmental area GABA projections pause accumbal cholinergic interneurons to enhance associative learning. Nature, 492(7429), 452–456. 10.1038/nature11657 [PubMed: 23178810]

Cachope R, Mateo Y, Mathur BN, Irving J, Wang HL, Morales M, … Cheer JF (2012). Selective activation of cholinergic interneurons enhances accumbal phasic dopamine release: Setting the tone for reward processing. Cell Reports, 2(1), 33–41. 10.1016/j.celrep.2012.05.011 [PubMed: 22840394]

Calabresi P, Lacey MG, & North RA (1989). Nicotine excitation of rat ventral tegmental neurones in vitro studied by intracellular recording. Br.J.Pharmacol, 98, 135–140. [PubMed: 2804543]

Capriles N, Rodaros D, Sorge RE, & Stewart J (2003). A role for the prefrontal cortex in stress- and cocaine-induced reinstatement of cocaine seeking in rats. Psychopharmacology, 168(1–2), 66–74. 10.1007/s00213-002-1283-z [PubMed: 12442201]

Carr DB, & Sesack SR (2000). Projections from the rat prefrontal cortex to the ventral tegmental area: target specificity in the synaptic associations with mesoaccumbens and mesocortical neurons. The Journal of Neuroscience, 20(10), 3864–3873. [PubMed: 10804226]

Chandler DJ, Lamperski CS, & Waterhouse BD (2013). Identification and distribution of projections from monoaminergic and cholinergic nuclei to functionally differentiated subregions of prefrontal cortex. Brain Research, 1522, 38–58. 10.1016/J.BRAINRES.2013.04.057 [PubMed: 23665053]

Chaudhury D, Walsh JJ, Friedman AK, Juarez B, Ku SM, Koo JW, … Han MH (2013). Rapid regulation of depression-related behaviours by control of midbrain dopamine neurons. Nature, 493(7433), 532–536. 10.1038/nature11713 [PubMed: 23235832]

Cohen JY, Haesler S, Vong L, Lowell BB, & Uchida N (2012). Neuron-type-specific signals for reward and punishment in the ventral tegmental area. Nature, 482(7383), 85–88. 10.1038/nature10754 [PubMed: 22258508]

Davis M (1992). The role of the amygdala in conditioned fear In The amygdala: Neurobiological aspects of emotion, memory, and mental dysfunction. (pp. 255–306). New York, NY, US: Wiley-Liss.

Deutch AY, & Cameron DS (1992). Pharmacalogical characterization of dopamine systems in the nucleus accumbens core and shell. Neuroscience, 46(1), 49–56. [PubMed: 1350665]

Deutch AY, Lee MC, Gillham MH, Cameron DA, Goldstein M, & Iadarola MJ (1991). Stress Selectively Increases Fos Protein in Dopamine Neurons Innervating the Prefrontal Cortex. Cerebral Cortex, 1(4), 273–292. 10.1093/cercor/1.4.273 [PubMed: 1668366]

Ding ZM, Ingraham CM, Rodd ZA, & McBride WJ (2015). The reinforcing effects of ethanol within the posterior ventral tegmental area depend on dopamine neurotransmission to forebrain cortico-limbic systems. Addiction Biology, 20(3), 458–468. 10.1111/adb.12138 [PubMed: 24674134]

Etkin A, Egner T, & Kalisch R (2011). Emotional processing in anterior cingulate and medial prefrontal cortex. Trends in Cognitive Sciences, 15(2), 85–93. 10.1016/j.tics.2010.11.004 [PubMed: 21167765]

Fallon JH (1981). Collateralization of monoamine neurons: mesotelencephalic dopamine projections to caudate, septum, and frontal cortex. J Neurosci, 1(12), 1361–1368. 10.1523/jneurosci.2521-09.2009 [PubMed: 6172572]

Fallon JH, & Moore RY (1978). Catecholamine innervation of the basal forebrain IV. Topography of the dopamine projection to the basal forebrain and neostriatum. Journal of Comparative Neurology, 180(3), 545–579. 10.1002/cne.901800310 [PubMed: 659674]

Fallon JH, Schmued LC, Wang C, Miller R, & Banales G (1984). Neurons in the ventral tegmentum have separate populations projecting to telencephalon and inferior olive, are histochemically different, and may receive direct visual input. Brain Research, 321(2), 332–336. 10.1016/0006-8993(84)90188-4 [PubMed: 6498523]

Fields HL, Hjelmstad GO, Margolis EB, & Nicola SM (2007). Ventral Tegmental Area Neurons in Learned Appetitive Behavior and Positive Reinforcement. Annual Review of Neuroscience, 30(1), 289–316. 10.1146/annurev.neuro.30.051606.094341

Flores JA, Galan-Rodriguez B, Ramiro-Fuentes S, & Fernandez-Espejo E (2006). Role for dopamine neurons of the rostral linear nucleus and periaqueductal gray in the rewarding and sensitizing properties of heroin. Neuropsychopharmacology, 31(7), 1475–1488. 10.1038/sj.npp.1300946 [PubMed: 16292327]

Floresco SB, Montes DR, Tse MMT, & van Holstein M (2018). Differential contributions of nucleus accumbens subregions to cue-guided risk/reward decision making and implementation of conditional rules. The Journal of Neuroscience, 38(8), 3191–17. 10.1523/JNEUROSCI.3191-17.2018

Gale SD, Person AL, & Perkel DJ (2008). A novel basal ganglia pathway forms a loop linking a vocal learning circuit with its dopaminergic input. The Journal of Comparative Neurology, 508(5), 824–839. 10.1002/cne.21700 [PubMed: 18398824]

Gallagher M (2000). The amygdala and associative learning The amygdala: A functional analysis. Oxford University Press.

Gong W, Neill D, & Justice JB (1996). Conditioned place preference and locomotor activation produced by injection of psychostimulants into ventral pallidum. Brain Research, 707(1), 64–74. 10.1016/0006-8993(95)01222-2 [PubMed: 8866714]

Gorelova N, Mulholland PJ, Chandler LJ, & Seamans JK (2012). The Glutamatergic Component of the Mesocortical Pathway Emanating from Different Subregions of the Ventral Midbrain. Cerebral Cortex, 22(2), 327–336. 10.1093/cercor/bhr107 [PubMed: 21666135]

Gourley SL, & Taylor JR (2016). Going and stopping: Dichotomies in behavioral control by the prefrontal cortex. Nature Neuroscience, 19(6), 656–664. 10.1038/nn.4275 [PubMed: 29162973]

Grove EA (1988). Neural associations of the substantia innominata in the rat: Afferent connections. Journal of Comparative Neurology, 277(3), 315–346. 10.1002/cne.902770302 [PubMed: 2461972]

Gunaydin LA, Grosenick L, Finkelstein JC, Kauvar IV, Fenno LE, Adhikari A, … Deisseroth K (2014). Natural neural projection dynamics underlying social behavior. Cell, 157(7), 1535–1551. 10.1016/j.cell.2014.05.017 [PubMed: 24949967]

Harris GC, & Aston-Jones G (2003). Critical role for ventral tegmental glutamate in preference for a cocaine-conditioned environment. Neuropsychopharmacology, 28(1), 73–76. 10.1038/sj.npp.1300011 [PubMed: 12496942]

Harris GC, Wimmer M, Byrne R, & Aston-Jones G (2004). Glutamate-associated plasticity in the ventral tegmental area is necessary for conditioning environmental stimuli with morphine. Neuroscience, 129(3), 841–847. 10.1016/j.neuroscience.2004.09.018 [PubMed: 15541905]

Hjelmstad GO, Xia Y, Margolis EB, & Fields HL (2013). Opioid modulation of ventral pallidal afferents to ventral tegmental area neurons. The Journal of Neuroscience, 33(15), 6454–6459. 10.1523/JNEUROSCI.0178-13.2013 [PubMed: 23575843]

Hnasko TS, Hjelmstad GO, Fields HL, & Edwards RH (2012). Ventral Tegmental Area Glutamate Neurons: Electrophysiological Properties and Projections. Journal of Neuroscience, 32(43), 15076–15085. 10.1523/JNEUROSCI.3128-12.2012 [PubMed: 23100428]

Hnasko TS, Sotak BN, & Palmiter RD (2005). Morphine reward in dopamine-deficient mice. Nature, 438(7069), 854–857. 10.1038/nature04172 [PubMed: 16341013]

Hubner CB, & Koob GF (1990). The ventral pallidum plays a role in mediating cocaine and heroin self-administration in the rat. Brain Res, 508(1), 20–9. [PubMed: 2337788]

Ikemoto S (2007). Dopamine reward circuitry: Two projection systems from the ventral midbrain to the nucleus accumbens–olfactory tubercle complex. Brain Research Reviews, 56(1), 27–78. 10.1016/J.BRAINRESREV.2007.05.004 [PubMed: 17574681]

Ikemoto S (2010). Brain reward circuitry beyond the mesolimbic dopamine system: A neurobiological theory. Neuroscience & Biobehavioral Reviews, 35(2), 129–150. 10.1016/j.neubiorev.2010.02.001 [PubMed: 20149820]

Ikemoto S, Qin M, & Liu Z-H (2006). Primary Reinforcing Effects of Nicotine Are Triggered from Multiple Regions Both Inside and Outside the Ventral Tegmental Area. J. Neurosci, 26(3), 723–730. 10.1523/jneurosci.4542-05.2006 [PubMed: 16421292]

Ikemoto S, Quin M, & Liu ZH (2005). The Functional Divide for Primary Reinforcement of D-Amphetamine Lies between the Medial and Lateral Ventral Striatum: Is the Division of the Accumbens Core, Shell, and Olfactory Tubercle Valid? Journal of Neuroscience, 25(20), 5061–5065. 10.1523/JNEUROSCI.0892-05.2005 [PubMed: 15901788]

Ilango A, Kesner AJ, Keller KL, Stuber GD, Bonci A, & Ikemoto S (2014). Similar Roles of Substantia Nigra and Ventral Tegmental Dopamine Neurons in Reward and Aversion. The Journal of Neuroscience. 10.1523/JNEUROSCI.1703-13.2014

Ito R, Robbins TW, & Everitt BJ (2004). Differential control over cocaine-seeking behavior by nucleus accumbens core and shell. Nature Neuroscience, 7(4), 389–397. 10.1038/nn1217 [PubMed: 15034590]

Johnson SW, & North RA (1992). Opioids excite dopamine neurons by hyperpolarization of local interneurons. The Journal of Neuroscience, 12(2), 483–488. [PubMed: 1346804]

Kantak KM, Black Y, Valencia E, Green-Jordan K, & Eichenbaum HB (2002). Dissociable Effects of Lidocaine Inactivation of the Rostral and Caudal Basolateral Amygdala on the Maintenance and Reinstatement of Cocaine-Seeking Behavior in Rats. Journal of Neuroscience, 22(3).

Kim J, Pignatelli M, Xu S, Itohara S, & Tonegawa S (2016). Antagonistic negative and positive neurons of the basolateral amygdala. Nature Neuroscience, 19(12), 1636–1646. 10.1038/nn.4414 [PubMed: 27749826]

Kirouac GJ, Li S, & Mabrouk G (2004). GABAergic projection from the ventral tegmental area and substantia nigra to the periaqueductal gray region and the dorsal raphe nucleus. The Journal of Comparative Neurology, 469(2), 170–184. 10.1002/cne.11005 [PubMed: 14694532]

Kirouac GJ, & Pittman QJ (2000). A projection from the ventral tegmental area to the periaqueductal gray involved in cardiovascular regulation. American Journal of Physiology-Regulatory, Integrative and Comparative Physiology, 278(6), R1643–R1650. 10.1152/ajpregu.2000.278.6.R1643

Klitenick MA, Eutch AY, Churchill L, & Kalivas PW (1992). Topography and functional role of dopaminergic projections from teh ventral mesenchephalic tegmentum to the ventral pallidum. Neuroscience, 50(2), 371–386. [PubMed: 1279461]

Kruzich PJ, & See RE (2001). Differential contributions of the basolateral and central amygdala in the acquisition and expression of conditioned relapse to cocaine-seeking behavior. The Journal of Neuroscience, 21, RC155 https://doi.org/20015433 [pii] [PubMed: 11425882]

Lammel S, Hetzel A, Häckel O, Jones I, Liss B, & Roeper J (2008). Unique Properties of Mesoprefrontal Neurons within a Dual Mesocorticolimbic Dopamine System. Neuron, 57(5), 760–773. 10.1016/j.neuron.2008.01.022 [PubMed: 18341995]

Lammel S, Lim BK, & Malenka RC (2014). Reward and aversion in a heterogeneous midbrain dopamine system. Neuropharmacology, 76, 351–359. 10.1016/J.NEUROPHARM.2013.03.019 [PubMed: 23578393]

Lammel S, Lim BK, Ran C, Huang KW, Betley MJ, Tye KM, … Malenka RC (2012). Input-specific control of reward and aversion in the ventral tegmental area. Nature, 491(7423), 212–217. 10.1038/nature11527 [PubMed: 23064228]

LeDoux J (1996). Emotional networks and motor control: a fearful view, 107, 437–446. 10.1016/S0079-6123(08)61880-4

Li X, Qi J, Yamaguchi T, Wang HL, & Morales M (2013). Heterogeneous composition of dopamine neurons of the rat A10 region: Molecular evidence for diverse signaling properties. Brain Structure and Function, 218(5), 1159–1176. 10.1007/s00429-012-0452-z [PubMed: 22926514]

Loughlin SE, & Fallon JH (1983). Dopaminergic and non-dopaminergic projections to amygdala from substantia nigra and ventral tegmental area. Brain Research, 262(2), 334–338. 10.1016/0006-8993(83)91029-6 [PubMed: 6839161]

Loughlin SE, & Fallon JH (1984). Substantia nigra and ventral tegmental area projections to cortex: Topography and collateralization. Neuroscience, 11(2), 425–435. 10.1016/0306-4522(84)90034-4 [PubMed: 6201780]

Margolis EB, Coker AR, Driscoll JR, Lemaître A-I, & Fields HL (2010). Reliability in the Identification of Midbrain Dopamine Neurons. PLoS ONE, 5(12), e15222 10.1371/journal.pone.0015222 [PubMed: 21151605]

Margolis EB, Lock H, Chefer VI, Shippenberg TS, Hjelmstad GO, & Fields HL (2006). Kappa opioids selectively control dopaminergic neurons projecting to the prefrontal cortex. Proceedings of the National Academy of Sciences of the United States of America, 103(8), 2938–2942. 10.1073/pnas.0511159103 [PubMed: 16477003]

Margolis EB, Lock H, Hjelmstad GO, & Fields HL (2006). The ventral tegmental area revisited: Is there an electrophysiological marker for dopaminergic neurons? Journal of Physiology, 577(3), 907–924. 10.1113/jphysiol.2006.117069 [PubMed: 16959856]

Margolis EB, Mitchell JM, Ishikawa J, Hjelmstad GO, & Fields HL (2008). Midbrain Dopamine Neurons: Projection Target Determines Action Potential Duration and Dopamine D2 Receptor Inhibition. Journal of Neuroscience, 28(36), 8908–8913. 10.1523/JNEUROSCI.1526-08.2008 [PubMed: 18768684]

Margolis EB, Toy B, Himmels P, Morales M, & Fields HL (2012). Identification of Rat Ventral Tegmental Area GABAergic Neurons. PLoS ONE, 7(7), e42365 10.1371/journal.pone.0042365 [PubMed: 22860119]

Maurice N, Deniau JM, Menetrey A, Glowinski J, & Thierry AM (1997). Position of the ventral pallidum in the rat prefrontal cortex basal ganglia circuit. Neuroscience, 80(2), 523–534. [PubMed: 9284354]

McBride WJ, Murphy JM, & Ikemoto S (1999). Localization of brain reinforcement mechanisms: Intracranial self-administration and intracranial place-conditioning studies. Behavioural Brain Research, 101(2), 129–152. 10.1016/S0166-4328(99)00022-4 [PubMed: 10372570]

McGaugh JL (2002). Memory consolidation and the amygdala: A systems perspective. Trends in Neurosciences, 25(9), 456–461. 10.1016/S0166-2236(02)02211-7 [PubMed: 12183206]

McLaughlin RJ, & Floresco SB (2007). The role of different subregions of the basolateral amygdala in cue-induced reinstatement and extinction of food-seeking behavior. Neuroscience, 146(4), 1484–1494. 10.1016/J.NEUROSCIENCE.2007.03.025 [PubMed: 17449185]

Meil WM, & See RE (1997). Lesions of the basolateral amygdala abolish the ability of drug associated cues to reinstate responding during withdrawal from self-administered cocaine. Behavioural Brain Research, 87(2), 139–148. 10.1016/S0166-4328(96)02270-X [PubMed: 9331482]

Millan MJ (2002). Descending control of pain. Progress in Neurobiology, 66(6), 355–474.10.1016/S0301-0082(02)00009-6 [PubMed: 12034378]

Moore RY, & Bloom FE (1978). Central Catecholamine Neuron Systems: Anatomy and Physiology of the Dopamine System. Annual Review of Neuroscience, 1, 129–169.

Moorman DE, James MH, McGlinchey EM, & Aston-Jones G (2015). Differential roles of medial prefrontal subregions in the regulation of drug seeking. Brain Research, 1628, 130–146. 10.1016/j.brainres.2014.12.024 [PubMed: 25529632]

Morales M, & Margolis EB (2017). Ventral tegmental area: cellular heterogeneity, connectivity and behaviour. Nature Reviews Neuroscience, 18(2), 73–85. 10.1038/nrn.2016.165 [PubMed: 28053327]

Morales M, & Root DH (2014). Glutamate neurons within the midbrain dopamine regions. Neuroscience, 282, 60–68. 10.1016/j.neuroscience.2014.05.032 [PubMed: 24875175]

Motta SC, Carobrez AP, & Canteras NS (2017). The periaqueductal gray and primal emotional processing critical to influence complex defensive responses, fear learning and reward seeking. Neuroscience and Biobehavioral Reviews, 76, 39–47. 10.1016/j.neubiorev.2016.10.012 [PubMed: 28434586]

Nader K, & van der Kooy D (1997). Deprivation state switches the neurobiological substrates mediating opiate reward in the ventral tegmental area. The Journal of Neuroscience, 17(1), 383–390. [PubMed: 8987763]

Narita M, Matsushima Y, Niikura K, Narita M, Takagi S, Nakahara K, … Suzuki T (2010). Implication of dopaminergic projection from the ventral tegmental area to the anterior cingulate cortex in μ-opioid-induced place preference. Addiction Biology, 15(4), 434–447. 10.1111/j.1369-1600.2010.00249.x [PubMed: 20731628]

Olmstead MC, & Franklin KBJ (1997). The development of a conditioned place preference to morphine: Effects of microinjections into various CNS sites. Behavioral Neuroscience, 111(6), 1324–1334. 10.1037/0735-7044.111.6.1324 [PubMed: 9438801]

Omelchenko N, & Sesack SR (2009). Ultrastructural analysis of local collaterals of rat ventral tegmental area neurons: GABA phenotype and synapses onto dopamine and GABA cells. Synapse, 63(10), 895–906. 10.1002/syn.20668 [PubMed: 19582784]

Omelchenko N, & Sesack SR (2010). Periaqueductal gray afferents synapse onto dopamine and GABA neurons in the rat ventral tegmental area. Journal of Neuroscience Research, 88(5), 981–991. 10.1002/jnr.22265 [PubMed: 19885830]

Paxinos G, & Watson C (1998). The Rat Brain in Stereotaxic Coordinates (4th ed.). Academic Press.

Pecina S, & Berridge KC (2005). Hedonic Hot Spot in Nucleus Accumbens Shell: Where Do-Opioids Cause Increased Hedonic Impact of Sweetness? Journal of Neuroscience, 25(50), 11777–11786. 10.1523/JNEUROSCI.2329-05.2005 [PubMed: 16354936]

Pecina S, & Berridge KC (2013). Dopamine or opioid stimulation of nucleus accumbens similarly. European Journal of Neuroscience, 37(9), 1529–1540. [PubMed: 23495790]

Peters J, LaLumiere RT, & Kalivas PW (2008). Infralimbic prefrontal cortex is responsible for inhibiting cocaine seeking in extinguished rats. The Journal of Neuroscience, 28(23), 6046–6053. 10.1523/JNEUROSCI.1045-08.2008 [PubMed: 18524910]

Pierce RC, & Kumaresan V (2006). The mesolimbic dopamine system: The final common pathway for the reinforcing effect of drugs of abuse? Neuroscience & Biobehavioral Reviews, 30(2), 215–238. 10.1016/J.NEUBIOREV.2005.04.016 [PubMed: 16099045]

Poulin J, Caronia G, Hofer C, Cui Q, Helm B, & Awatramani R (2018). Mapping projections of molecularly defined dopamine neuron subtypes using intersectional genetic approaches. Nature Neuroscience. 10.1038/s41593-018-0203-4

Qi J, Zhang S, Wang H, Barker DJ, Miranda-barrientos J, & Morales M (2016). VTA glutamatergic inputs to nucleus accumbens drive aversion by acting on GABAergic interneurons. Nature Neuroscience, 19(5), 725–733. 10.1038/nn.4281.VTA [PubMed: 27019014]

Richard JM, Ambroggi F, Janak PH, & Fields HL (2016). Ventral Pallidum Neurons Encode Incentive Value and Promote Cue-Elicited Instrumental Actions. Neuron, 90(6), 1165–1173. 10.1016/j.neuron.2016.04.037 [PubMed: 27238868]

Rodríguez-López C, Clascá F, & Prensa L (2017). The Mesoaccumbens Pathway: A Retrograde Labeling and Single-Cell Axon Tracing Analysis in the Mouse. Frontiers in Neuroanatomy, 11, 25 10.3389/fnana.2017.00025 [PubMed: 28396627]

Root DH, Mejias-Aponte C, Zhang S, Wang H, Hoffman A, Lupica CR, & Morales M (2014). Single rodent mesohabenular axons release glutamate and GABA. Nature Neuroscience, 17(11), 1–21. [PubMed: 24369367]

Root DH, Melendez RI, Zaborszky L, & Napier TC (2015). The ventral pallidum: Subregion-specific functional anatomy and roles in motivated behaviors. Progress in Neurobiology, 130, 29–70. 10.1016/j.pneurobio.2015.03.005 [PubMed: 25857550]

Root DH, Wang H-L, Liu B, Barker DJ, Mód L, Szocsics P, … Morales M (2016). Glutamate neurons are intermixed with midbrain dopamine neurons in nonhuman primates and humans. Scientific Reports, 6(1), 30615 10.1038/srep30615 [PubMed: 27477243]

Root DH, Zhang S, Barker DJ, Miranda-Barrientos J, Liu B, Wang HL, & Morales M (2018). Selective Brain Distribution and Distinctive Synaptic Architecture of Dual Glutamatergic-GABAergic Neurons. Cell Reports. 10.1016/j.celrep.2018.05.063

Rushworth MFS, Walton ME, Kennerley SW, & Bannerman DM (2004). Action sets and decisions in the medial frontal cortex. Trends in Cognitive Sciences, 8(9), 410–417. 10.1016/j.tics.2004.07.009 [PubMed: 15350242]

Salamone JD, & Correa M (2012). The Mysterious Motivational Functions of Mesolimbic Dopamine. Neuron, 76(3), 470–485. 10.1016/j.neuron.2012.10.021 [PubMed: 23141060]

Salamone JD, Correa M, Mingote SM, & Weber SM (2005). Beyond the reward hypothesis: Alternative functions of nucleus accumbens dopamine. Current Opinion in Pharmacology, 5(1), 34–41. 10.1016/j.coph.2004.09.004 [PubMed: 15661623]

Sanchez-Catalan MJ, Kaufling J, Georges F, Veinante P, & Barrot M (2014). The antero-posterior heterogeneity of the ventral tegmental area. Neuroscience, 282, 198–216. 10.1016/J.NEUROSCIENCE.2014.09.025 [PubMed: 25241061]

Saunders BT, Richard JM, Margolis EB, & Janak PH (2018). Dopamine neurons create Pavlovian conditioned stimuli with circuit-defined motivational properties. Nature Neuroscience 10.1038/s41593-018-0191-4

Schweimer J, & Hauber W (2005). Involvement of the rat anterior cingulate cortex in control of instrumental responses guided by reward expectancy. Learning & Memory, 12(3), 334–342. 10.1101/lm.90605 [PubMed: 15930509]

Seroogy KB, Dangaran K, Lim S, Haycock JW, & Fallon JH (1989). Ventral mesencephalic neurons containing both cholecystokinin- and tyrosine hydroxylase-like immunoreactivities project to forebrain regions. The Journal of Comparative Neurology, 279(3), 397–414. 10.1002/cne.902790306 [PubMed: 2563737]

Shin R, Qin M, Liu ZH, & Ikemoto S (2008). Intracranial self-administration of MDMA into the ventral striatum of the rat: Differential roles of the nucleus accumbens shell, core, and olfactory tubercle. Psychopharmacology, 198(2), 261–270. 10.1007/s00213-008-1131-x [PubMed: 18389222]

Smith KS, Tindell AJ, Aldridge JW, & Berridge KC (2009). Ventral pallidum roles in reward and motivation. Behavioural Brain Research, 196(2), 155–167. 10.1016/j.bbr.2008.09.038 [PubMed: 18955088]

Steinberg EE, Boivin JR, Saunders BT, Witten IB, Deisseroth K, & Janak PH (2014). Positive reinforcement mediated by midbrain dopamine neurons requires D1 and D2 receptor activation in the nucleus accumbens. PLoS ONE, 9(4). 10.1371/journal.pone.0094771

Stuber GD, Hnasko TS, Britt JP, Edwards RH, & Bonci A (2010). Dopaminergic Terminals in the Nucleus Accumbens But Not the Dorsal Striatum Corelease Glutamate. Journal of Neuroscience, 30(24), 8229–8233. 10.1523/JNEUROSCI.1754-10.2010 [PubMed: 20554874]

Swanson LW (1982). The Projections of the Ventral Tegmental Area and Adjacent Regions: A Combined Fluorescent Retrograde Tracer and Immunofluorescence Study in the Rat. Brain Research Bulletin, 9, 321–353. [PubMed: 6816390]

Tan KR, Yvon C, Turiault M, Mirzabekov JJ, Doehner J, Labouèbe G, … Lüscher C (2012). GABA Neurons of the VTA Drive Conditioned Place Aversion. Neuron, 73(6), 1173–1183. 10.1016/J.NEURON.2012.02.015 [PubMed: 22445344]

Taylor SR, Badurek S, Dileone RJ, Nashmi R, Minichiello L, & Picciotto MR (2014). GABAergic and glutamatergic efferents of the mouse ventral tegmental area. Journal of Comparative Neurology, 522(14), 3308–3334. 10.1002/cne.23603 [PubMed: 24715505]

Tecuapetla F, Patel JC, Xenias H, English D, Tadros I, Shah F, … Koos T (2010). Glutamatergic Signaling by Mesolimbic Dopamine Neurons in the Nucleus Accumbens. Journal of Neuroscience, 30(20), 7105–7110. 10.1523/JNEUROSCI.0265-10.2010 [PubMed: 20484653]

Threlfell S, & Cragg SJ (2011). Dopamine Signaling in Dorsal Versus Ventral Striatum: The Dynamic Role of Cholinergic Interneurons. Frontiers in Systems Neuroscience, 5(March), 1–10. 10.3389/fnsys.2011.00011 [PubMed: 21347218]

Tsai HC, Zhang F, Adamantidis A, Stuber GD, Bond A, De Lecea L, & Deisseroth K (2009). Phasic firing in dopaminergic neurons is sufficient for behavioral conditioning. Science, 324(5930), 1080–1084. 10.1126/science.1168878 [PubMed: 19389999]

Tzschentke TM (2000). The medial prefrontal cortex as a part of the brain reward system Review Article. Amino Acid, 19, 211–219. 10.1007/s007260070051

Van Bockstaele EJ, & Pickel VM (1995). GABA-containing neurons in the ventral tegmental area project to the nucleus accumbens in rat brain. Brain Research, 682(1–2), 215–221. 10.1016/0006-8993(95)00334-M [PubMed: 7552315]

Van Zessen R, Phillips JL, Budygin EA, & Stuber GD (2012). Activation of VTA GABA Neurons Disrupts Reward Consumption. Neuron, 73(6), 1184–1194. 10.1016/j.neuron.2012.02.016 [PubMed: 22445345]

Vidal-Gonzalez I, Vidal-Gonzalez B, Rauch SL, & Quirk GJ (2006). Microstimulation reveals opposing influences of prelimbic and infralimbic cortex on the expression of conditioned fear. Learning & Memory (Cold Spring Harbor, N.Y.), 13(6), 728–733. 10.1101/lm.306106

Volkow ND, Wise RA, & Baler R (2017). The dopamine motive system: Implications for drug and food addiction. Nature Reviews Neuroscience, 18(12), 741–752. 10.1038/nrn.2017.130 [PubMed: 29142296]

Walton ME, Bannerman DM, Alterescu K, & Rushworth MFS (2003). Functional specialization within medial frontal cortex of the anterior cingulate for evaluating effort-related decisions. The Journal of Neuroscience, 23(16), 6475–6479. https://doi.org/23/16/6475 [pii] [PubMed: 12878688]

Williams JT, North RA, Shefner SA, Nishi S, & Egan TM (1984). Membrane properties of rat locus coeruleus neurones. Neuroscience, 13(1), 137–156. 10.1016/0306-4522(84)90265-3 [PubMed: 6493483]

Wise RA, & Rompre PP (1989). Brain Dopamine and Reward. Annual Review of Psychology, 40(1), 191–225. 10.1146/annurev.ps.40.020189.001203

Witten IB, Steinberg EE, Lee SY, Davidson TJ, Zalocusky KA, Brodsky M, … Deisseroth K (2011). Recombinase-driver rat lines: Tools, techniques, and optogenetic application to dopamine-mediated reinforcement. Neuron, 72(5), 721–733. 10.1016/j.neuron.2011.10.028 [PubMed: 22153370]

Wright CI, Beijer AV, & Groenewegen HJ (1996). Basal amygdaloid complex afferents to the rat nucleus accumbens are compartmentally organized. The Journal of Neuroscience, 16(5), 1877–1893. [PubMed: 8774456]

Yamaguchi T, Wang H-L, Li X, Ng TH, & Morales M (2011). Mesocorticolimbic glutamatergic pathway. The Journal of Neuroscience, 31(23), 8476–8490. 10.1523/JNEUROSCI.1598-11.2011 [PubMed: 21653852]

Yang K, Hu J, Lucero L, Liu Q, Zheng C, Zhen X, … Wu J (2009). Distinctive nicotinic acetylcholine receptor functional phenotypes of rat ventral tegmental area dopaminergic neurons. The Journal of Physiology, 587(2), 345–361. 10.1113/jphysiol.2008.162743 [PubMed: 19047205]

Zaborszky L, Gaykema RP, Swanson DJ, & Cullinan WE (1997). Cortical input to the basal forebrain. Neuroscience, 79(4), 1051–1078. 10.1016/S0306-4522(97)00049-3 [PubMed: 9219967]

Zahm DS (1998). Functional-anatomical implications of the nucleus accumbens core and shell subterritories. Annals of the New York Academy of Sciences, 877(1), 113–128. 10.1111/j.1749-6632.1999.tb09264.x

Zangen A, Ikemoto S, Zadina JE, & Wise RA (2002). Rewarding and psychomotor stimulant effects of endomorphin-1: anteroposterior differences within the ventral tegmental area and lack of effect in nucleus accumbens. J Neurosci, 22(16), 7225–7233. https://doi.org/20026722 [PubMed: 12177217]

Zhou FM, Liang Y, & Dani JA (2001). Endogenous nicotinic cholinergic activity regulates dopamine release in the striatum. Nature Neuroscience, 4(12), 1224–1229. 10.1038/nn769 [PubMed: 11713470]

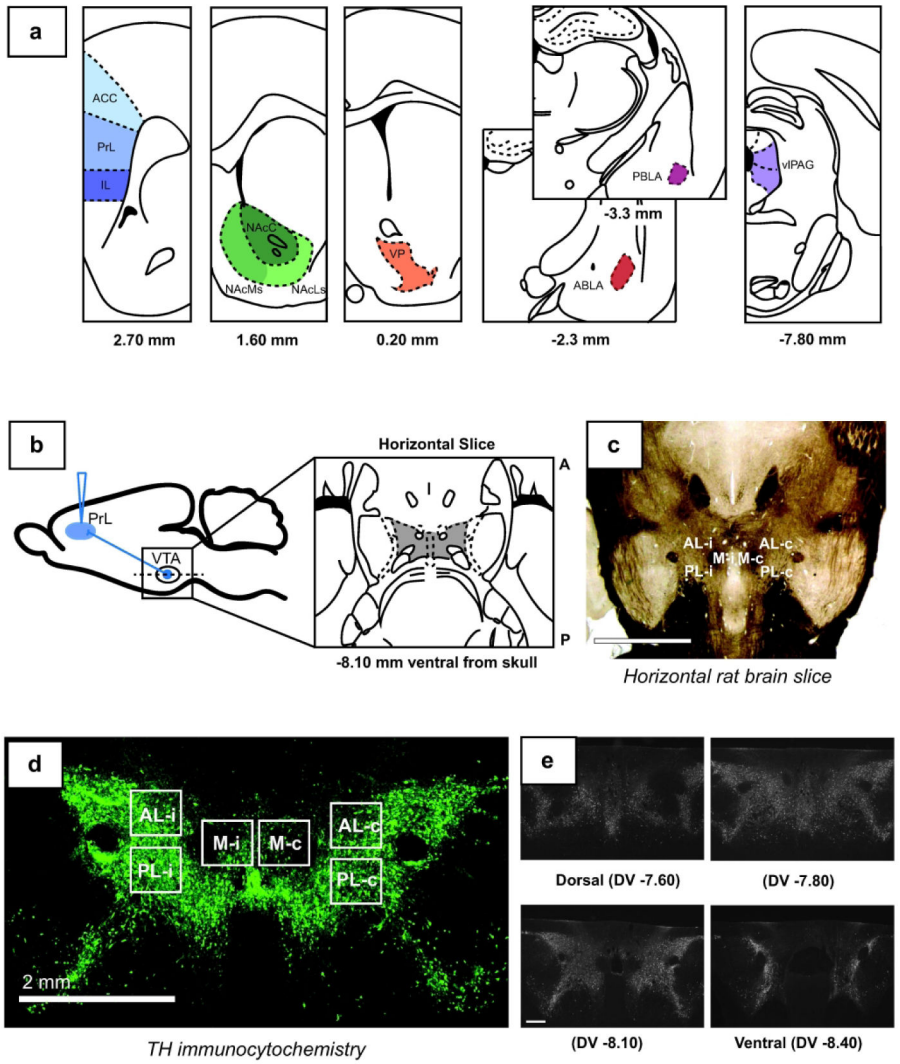

Figure 1.

Methods summary. (a) Representations of coronal sections of the target nuclei receiving retrograde tracer injections. Coordinates are anterior-posterior from bregma (Paxinos & Watson, 1998). For surgical coordinates, see Table 2. (b) Seven days after tracer injection (left), horizontal sections of the VTA were made for analysis of the distributions of retrogradely labeled neurons within the VTA (right) (−8.10 mm ventral from the skull surface) (Paxinos & Watson, 1998). (c) Example brightfield image of a horizontal slice containing the VTA, 50 μm thick. The sampling regions are indicated (−8.10 mm ventral) Scale bar 2 mm. (d) Fluorescent image of a horizontal slice containing the VTA, 50 μm thick, immunocytochemically labeled for TH (green) and depicting the sampling regions (−8.10 mm ventral). (e) Horizontal VTA slices immunocytochemically labeled for TH representing the dorsal-ventral (DV) extent of the VTA. Approximate coordinates are dorsal-ventral from the skull surface (Paxinos & Watson, 1998). Scale bar 500 μm.

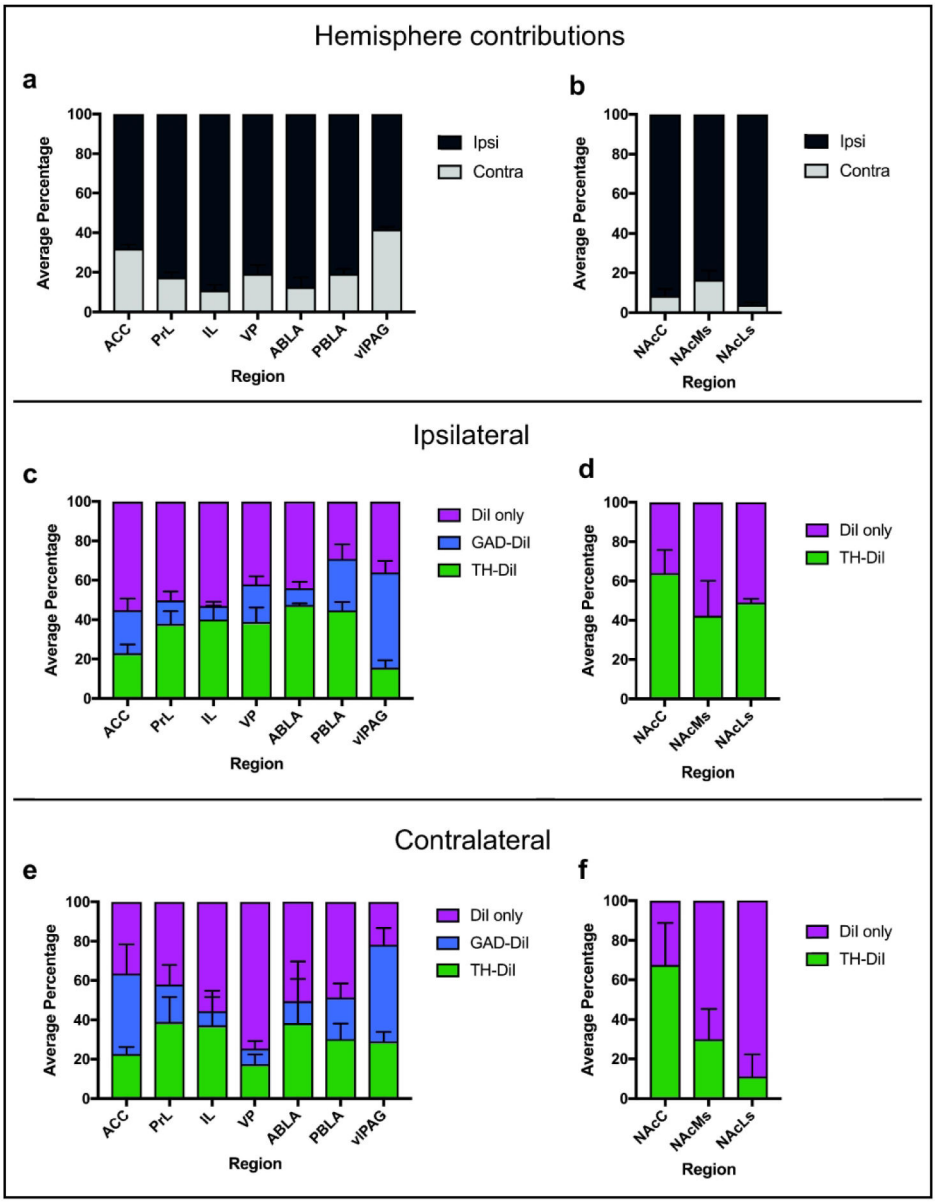

Figure 2.

Overall quantification of retrogradely labeled VTA neurons for each projection: laterality, and dopaminergic and GABAergic contributions. (a) Ipsilateral (ipsi) and contralateral (contra) VTA projection densities for ACC, PrL, IL, VP, ABLA, PBLA, and vlPAG. (b) Ipsilateral and contralateral VTA projection densities for NAcC, NAcMs, and NAcLs. (c) The proportions of ipsilateral retrogradely labeled neurons that were co-labeled with either TH (TH-DiI) or GAD (GAD-DiI) for ACC, PrL, IL, VP, ABLA, PBLA, and vlPAG. (d) The proportions of ipsilateral retrogradely labeled VTA neurons that project to the NAc sub-regions and were co-labeled for TH (TH-DiI). (e) The proportions of contralateral retrogradely labeled neurons that were co-labeled with either TH (TH-DiI) or GAD (GAD-DiI) for ACC, PrL, IL, VP, ABLA, PBLA, and vlPAG. (f) The proportions of contralateral

retrogradely labeled VTA neurons that project to the NAc sub-regions and were co-labeled for TH (TH-DiI). All results are presented as mean ± S.E.M.

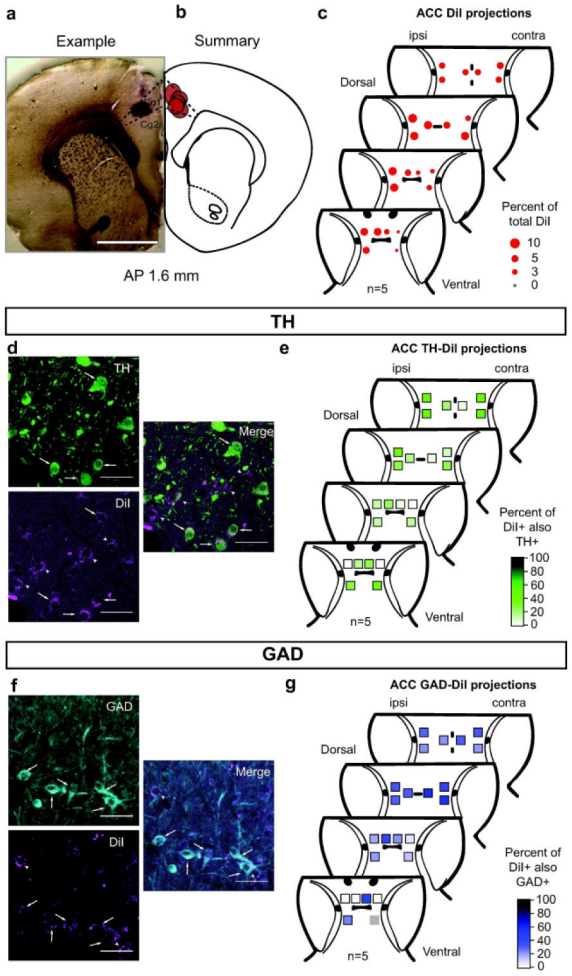

Figure 3.

Projections from the VTA to the anterior cingulate cortex (ACC). (a) Example DiI injection site in the ACC (AP 1.6 mm). Scale bar 2 mm. (b) Summary of all DiI injection sites (red circles) in the ACC (AP 1.6 mm) (Paxinos & Watson, 1998). n=5 (c) Retrogradely labeled neurons were detected in all sampling regions throughout the DV extent of the VTA. Dot size indicates the mean percentage of retrogradely labeled neurons within that sampling window compared to the total projection. The slice depths from dorsal to ventral are approximately −7.8, −8.0, −8.2 and −8.4 mm. (d) Example images of DiI labeled cells (magenta) and immunofluorescent labeling for TH (green). Scale bar 50 μm. Arrows indicate TH-DiI co-labeled neurons. Arrowheads indicate DiI only neurons. (e) Within each sampling region, the color indicates the percentage of DiI neurons co-labeled with TH. (f) Representative images of DiI filled cells and immunofluorescent labeling for GAD. Scale bar 50 μm. Arrows indicate GAD-DiI co-labeled neurons. Arrowheads represent DiI only neurons. (g) Within each sampling region, the color indicates the percentage of DiI neurons co-localized with GAD.

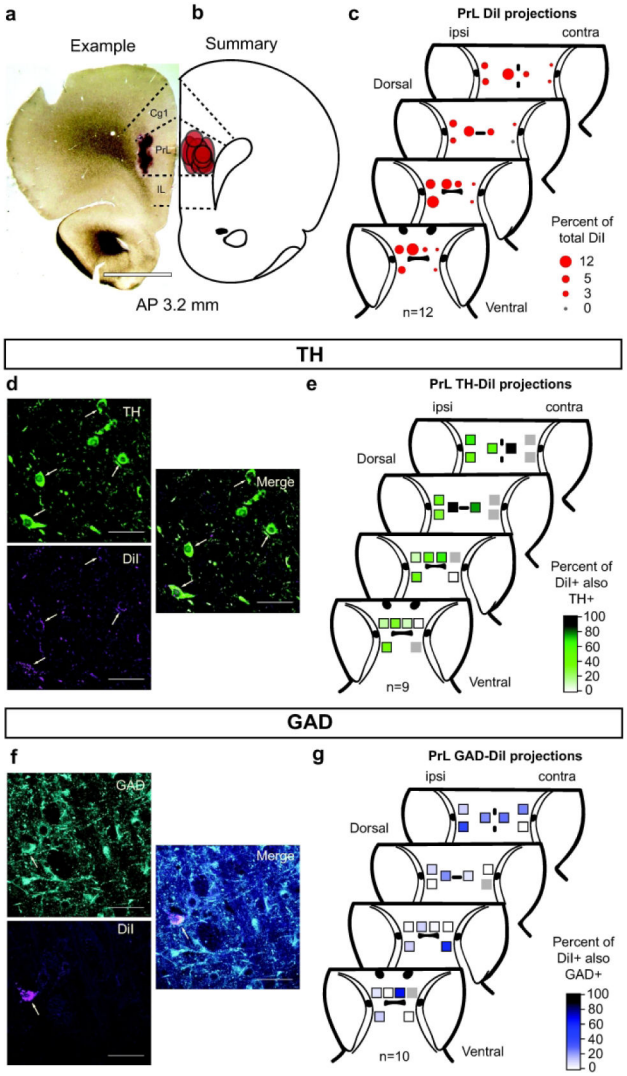

Figure 4.

Projections from the VTA to the prelimbic cortex (PrL). (a) Example DiI injection site in the PrL (AP 3.2 mm). Scale bar 2 mm. (b) Summary of all DiI injection sites (red circles) in the PrL (AP 3.2 mm) (Paxinos & Watson, 1998). n=12 (c) Retrogradely labeled neurons were detected in all but one sampling region throughout the DV extent of the VTA. Dot size indicates the mean percentage of retrogradely labeled neurons within that sampling window compared to the total projection. The slice depths from dorsal to ventral are approximately −7.8, −8.0, −8.2 and −8.4 mm. (d) Representative images of DiI labeled cells (magenta) and immunofluorescent labeling for TH (green). Scale bar 50 μm. Arrows indicate TH-DiI co-labeled neurons. (e) Within each sampling region, the color indicates the percentage of DiI neurons co-labeled with TH. (f) Representative images of DiI filled cells and immunofluorescent labeling for GAD. Scale bar 50 μm. Arrow indicates GAD-DiI co-labeled neuron. (g) Within each sampling region, the color indicates the percentage of DiI neurons co-localized with GAD.

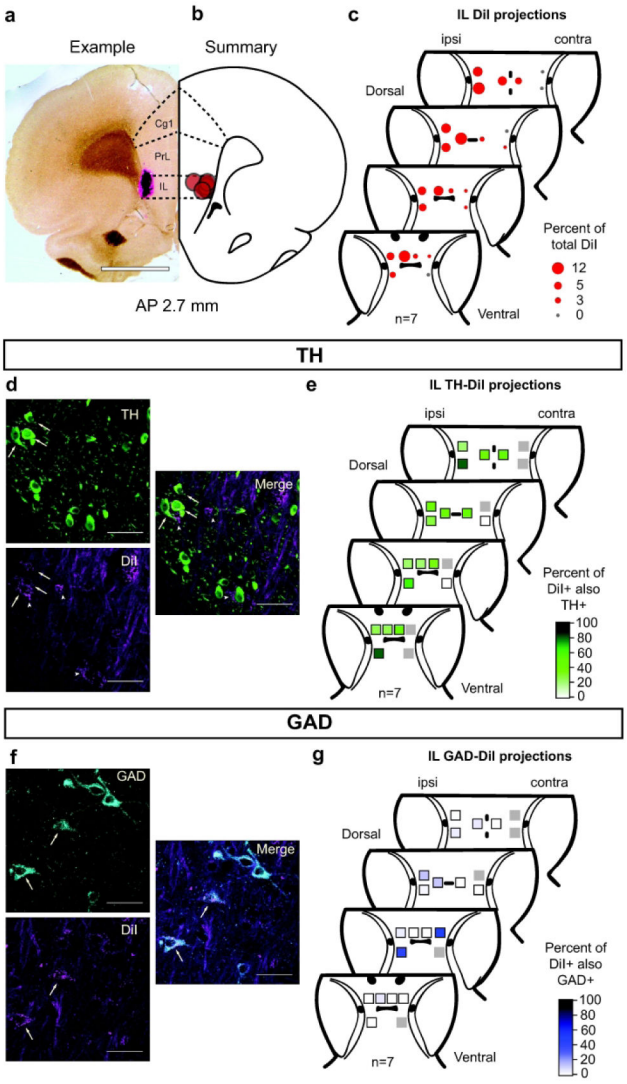

Figure 5.

Projections from the VTA to the infralimbic cortex (IL). (a) Example DiI injection site in the IL (AP 2.7 mm). Scale bar 2 mm (b) Summary of all DiI injection sites (red circles) in the IL (AP 2.7 mm) (Paxinos & Watson, 1998). n=7 (c) Retrogradely labeled neurons were detected in all sampling regions ipsilateral to the injection site throughout the DV extent of the VTA. Dot size indicates the mean percentage of retrogradely labeled neurons within that sampling window compared to the total projection. The slice depths from dorsal to ventral are approximately −7.8, −8.0, −8.2 and −8.4 mm. (d) Representative images of DiI filled cells (magenta) and immunofluorescent labeling for TH (green). Scale bar 50 μm. Arrows indicate TH-DiI co-labeled neurons. Arrowheads indicate DiI only neurons. (e) Within each sampling region, the color indicates the percentage of DiI neurons co-labeled with TH across animals. (f) Representative images of DiI filled cells and immunofluorescent labeling for GAD. Scale bar 50 μm. Arrows indicate GAD-DiI co-labeled neurons. (g) Within each sampling region, the color indicates the percentage of DiI neurons co-localized with GAD.

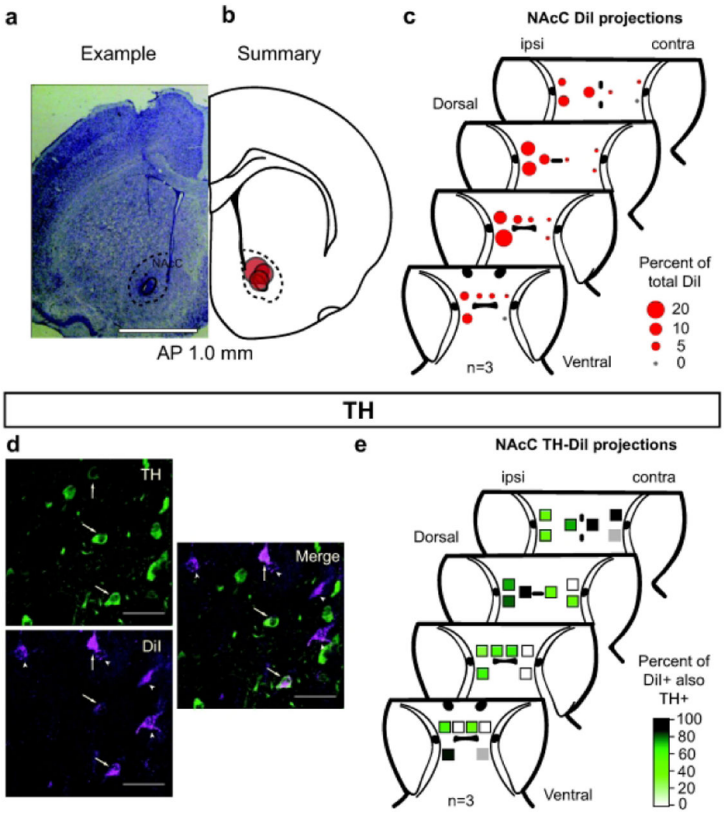

Figure 6.

Projections from the VTA to the nucleus accumbens core (NAcC). (a) Example DiI injection site in the NAcC (AP 1.0 mm). Scale bar 2 mm. (b) Summary of all DiI injection sites (red circles) in the NAcC (AP 1.0 mm) (Paxinos & Watson, 1998). n=3 (c) Retrogradely labeled neurons were detected in all but two sampling regions throughout the DV extent of the VTA. Dot size indicates the mean percentage of retrogradely labeled neurons within that sampling window compared to the total projection. The slice depths from dorsal to ventral are approximately −7.8, −8.0, −8.2 and −8.4 mm. (d) Representative images of DiI filled cells (magenta) and immunofluorescent labeling for TH (green). Scale bar 50 μm. Arrows indicate TH-DiI co-labeled neurons. Arrowheads indicate DiI only neurons. (e) Within each sampling region, the color indicates the percentage of DiI neurons co-labeled with TH.

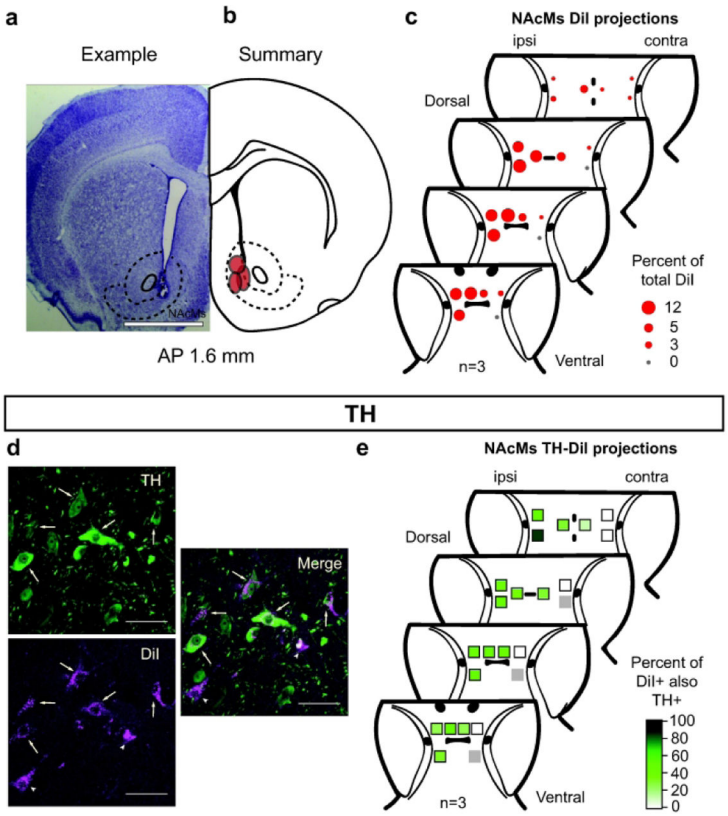

Figure 7.

Projections from the VTA to the nucleus accumbens medial shell (NAcMs). (a) Example DiI injection site in the NacMs (AP 1.6 mm). Scale bar 2 mm. (b) Summary of all DiI injection sites (red circles) in the NAcMs (AP 1.6 mm) (Paxinos & Watson, 1998). n=3 (c) Retrogradely labeled neurons were detected in all ipsilateral sampling regions throughout the DV extent of the VTA. Dot size indicates the mean percentage of retrogradely labeled neurons within that sampling window compared to the total projection. The slice depths from dorsal to ventral are approximately −7.8, −8.0, −8.2 and −8.4 mm. (d) Representative images of DiI filled cells (magenta) and immunofluorescent labeling for TH (green). Scale bar 50 μm. Arrows indicate TH-DiI co-labeled neurons. Arrowheads indicate DiI only neurons. (e) Within each sampling region, the color indicates the percentage of DiI neurons co-localized with TH.

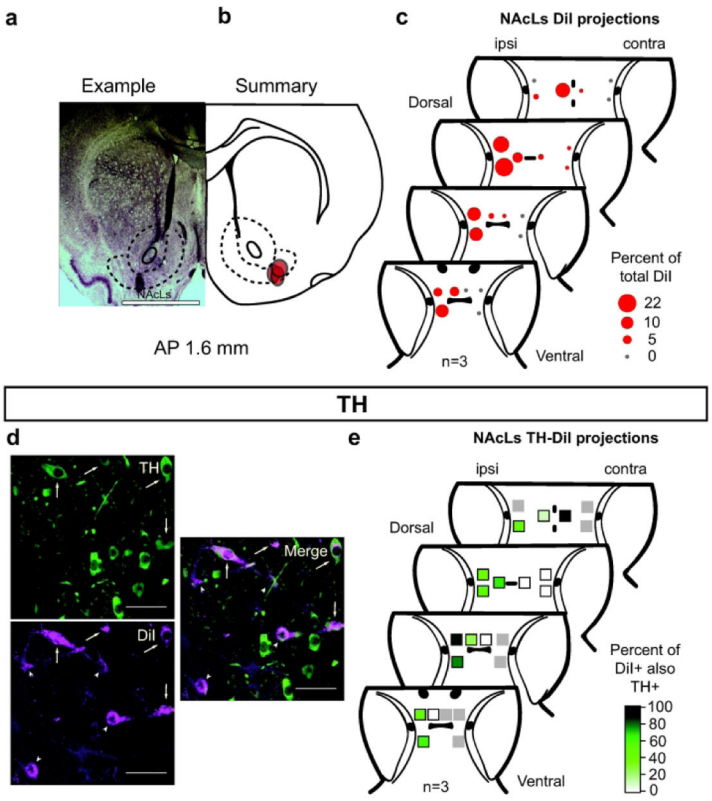

Figure 8.

Projections from the VTA to the nucleus accumbens lateral shell (NAcLs). (a) Example DiI injection site in the NAcLs (AP 1.6 mm). Scale bar 2mm. (b) Summary of all DiI injection sites (red circles) in the NAcLs (AP 1.6 mm) (Paxinos & Watson, 1998). n=3. (c) Retrogradely labeled neurons were detected in all sampling regions throughout the DV extent of the VTA. Dot size indicates the mean percentage of retrogradely labeled neurons within that sampling window compared to the total projection. The slice depth from dorsal to ventral is approximately −7.8, −8.0, −8.2 and −8.4 mm. (d) Representative images of DiI filled cells (magenta) and immunofluorescent labeling for TH (green). Scale bar 50 μm. Arrows indicate DiI, TH co-labeled neurons. Arrowheads indicate DiI(+), TH(−) neurons. (e) Within each sampling region, the color indicates the percentage of DiI neurons co-localized with TH.

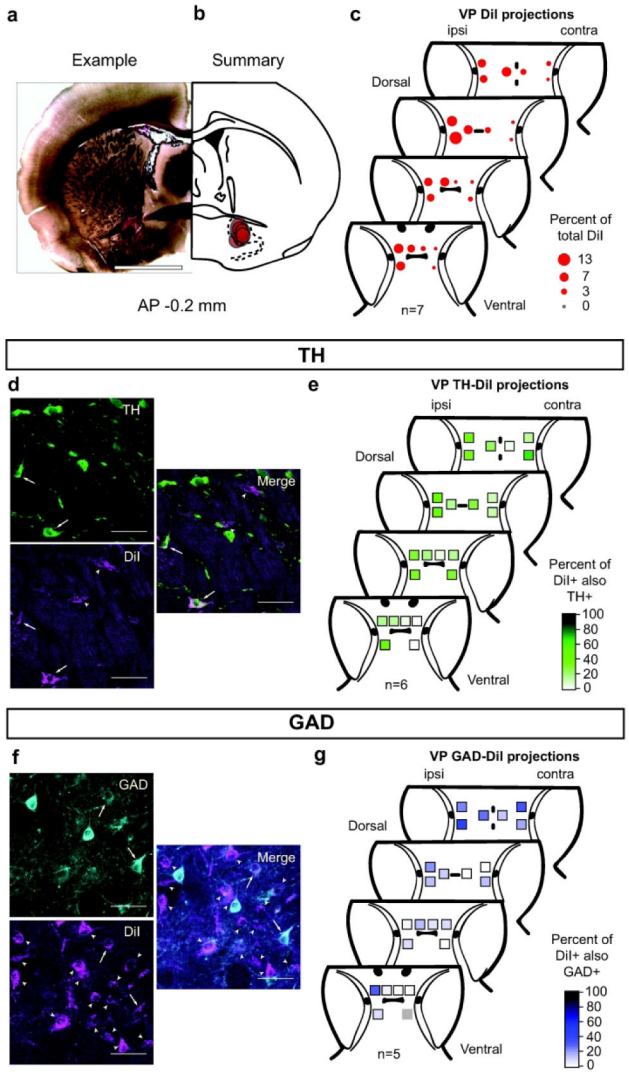

Figure 9.

Projections from the VTA to the ventral pallidum (VP). (a) Example DiI injection site in the VP (AP −0.2 mm). Scale bar 2 mm. (b) Summary of all DiI injection sites (red circles) in the VP (AP −0.2 mm) (Paxinos & Watson, 1998). n=7 (c) Retrogradely labeled neurons were detected in all sampling regions throughout the DV extent of the VTA. Dot size indicates the mean percentage of retrogradely labeled neurons within that sampling window compared to the total projection. The slice depths from dorsal to ventral are approximately −7.8, −8.0, −8.2 and −8.4 mm. (d) Representative images of DiI filled cells (magenta) and immunofluorescent labeling for TH (green). Scale bar 50 μm. Arrows indicate TH-DiI co-labeled neurons. Arrowheads indicate DiI only neurons. (e) Within each sampling region, the color indicates the percentage of DiI neurons co-labeled with TH. (f) Representative images of DiI filled cells and immunofluorescent labeling for GAD. Scale bar 50 μm. Arrows indicate GAD-DiI co-labeled neurons. Arrowheads represent DiI only neurons. (g) Within each sampling region, the color indicates the percentage of DiI neurons co-localized with GAD.

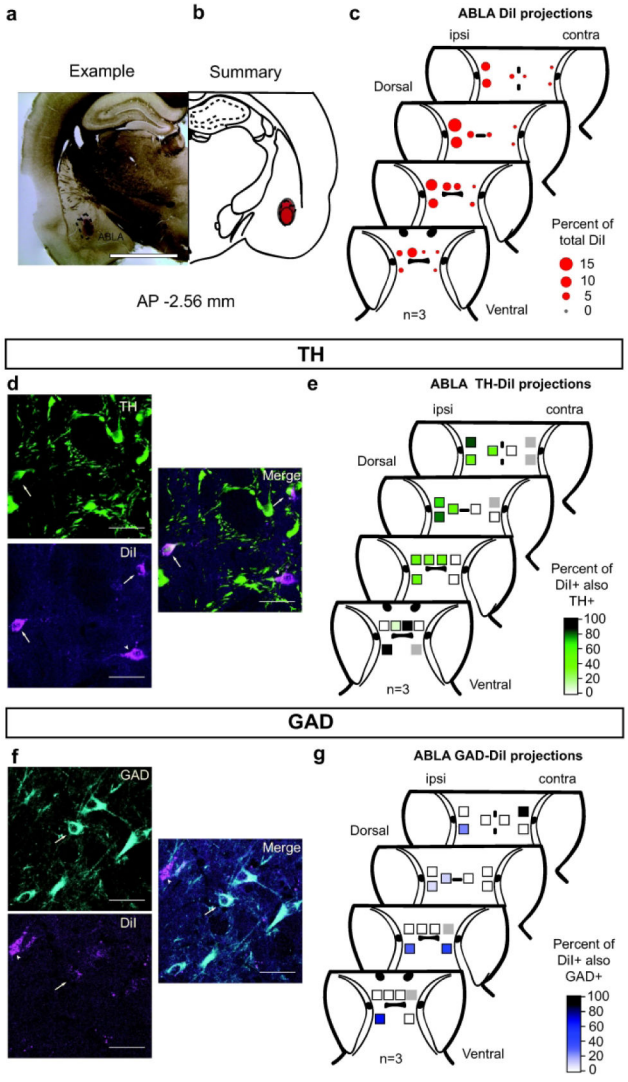

Figure 10.

Projections from the VTA to the anterior basolateral amygdala (ABLA). (a) Example DiI injection site in the ABLA (AP −2.56 mm). Scale bar 2 mm. (b) Summary of all DiI injection sites (red circles) in the ABLA (AP −2.56 mm) (Paxinos & Watson, 1998). n=3. (c) Retrogradely labeled neurons were detected in all sampling regions throughout the DV extent of the VTA. Dot size indicates the mean percentage of retrogradely labeled neurons within that sampling window compared to the total projection. The slice depths from dorsal to ventral are approximately −7.8, −8.0, −8.2 and −8.4 mm. (d) Representative images of DiI filled cells (magenta) and immunofluorescent labeling for TH (green). Scale bar 50 μm. Arrow indicates TH-DiI co-labeled neuron. Arrowheads indicate DiI only neurons. (e) Within each sampling region, the color indicates the percentage of DiI neurons co-labeled with TH. (f) Representative images of DiI filled cells and immunofluorescent labeling for GAD. Scale bar 50 μm. Arrows indicate GAD-DiI co-labeled neurons. Arrowhead represents DiI only neuron. (g) Within each sampling region, the color indicates the percentage of DiI neurons co-localized with GAD.

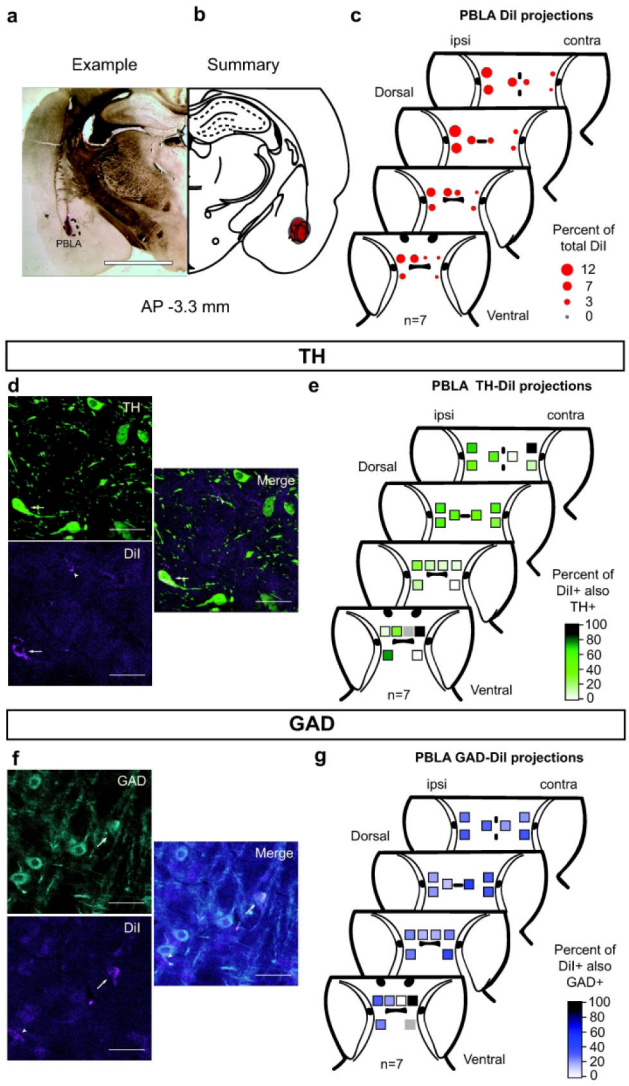

Figure 11.

Projections from the VTA to the posterior basolateral amygdala (PBLA). (a) Example DiI injection site in the PBLA (AP −3.3 mm) Scale bar 2 mm. (b) Summary of all DiI injection sites (red circles) in the PBLA (AP −3.3 mm) (Paxinos & Watson, 1998). n=7 (c) Retrogradely labeled neurons were detected in all sampling regions throughout the DV extent of the VTA. Dot size indicates the mean percentage of retrogradely labeled neurons within that sampling window compared to the total projection. The slice depths from dorsal to ventral are approximately −7.8, −8.0, −8.2 and −8.4 mm. (d) Representative images of DiI filled cells (magenta) and immunofluorescent labeling for TH (green). Scale bar 50 μm. Arrow indicates TH-DiI co-labeled neuron. Arrowhead indicates DiI only neuron. (e) Within each sampling region, the color indicates the percentage of DiI neurons co-labeled with TH. (f) Representative images of DiI filled cells and immunofluorescent labeling for GAD. Scale bar 50 μm. Arrow indicates GAD-DiI co-labeled neuron. Arrowhead represents DiI only neuron. (g) Within each sampling region, the color indicates the percentage of DiI neurons co-labeled with GAD.

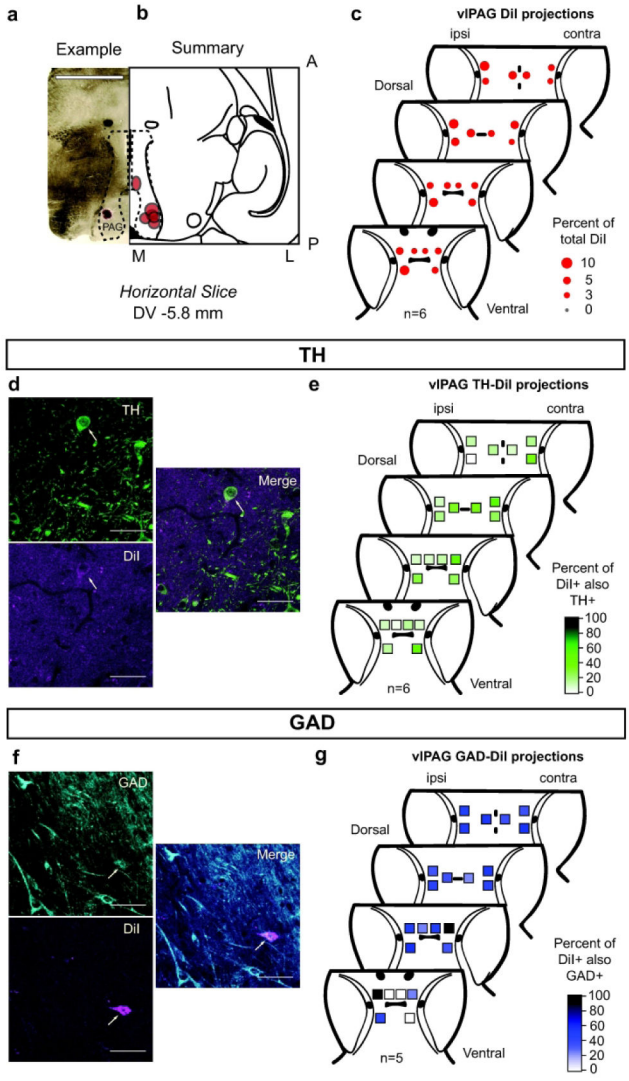

Figure 12.

Projections from the VTA to the ventrolateral periaqueductal gray (vlPAG). (a) Example DiI injection site in the vlPAG (DV −5.8 mm). Scale bar 2 mm. (b) Summary of all DiI injection sites (red circles) in the vlPAG (DV −5.8 mm) (Paxinos & Watson, 1998). n=6 (c) Retrogradely labeled neurons were distributed relatively evenly across both ipsilateral and contralateral sampling regions throughout the DV extent of the VTA. Dot size indicates the mean percentage of retrogradely labeled neurons within that sampling window compared to the total projection. The slice depths from dorsal to ventral are approximately −7.8, −8.0, −8.2 and −8.4 mm. (d) Representative images of DiI filled cells (magenta) and immunofluorescent labeling for TH (green). Scale bar 50 μm. Arrow indicates TH-DiI co-labeled neuron. (e) Within each sampling region, the color indicates the percentage of DiI neurons co-labeled with TH. (f) Representative images of DiI filled cells and immunofluorescent labeling for GAD. Scale bar 50 μm. Arrow indicates GAD-DiI co-labeled neuron. (g) Within each sampling region, the color indicates the percentage of DiI neurons co-localized with GAD.

TABLE 1.

Protocol details across animals.

Protocol Name	Tracer Injection Method	Perfusion Method	Image Collection	Number of Animals by target
A	Injection cannula connected to 1 ml Hamilton syringe	10% formalin	Zeiss LSM510 META	ACC: 4 PrL: 4 NAcC: 1 VP: 2 vlPAG: 3
B	Nanoject injector	4% paraformaldehyde	Zeiss Axioskop 2	ACC: 1 PrL: 5 IL: 7 NAcC: 2 NAcMs: 3 NAcLs: 3 VP: 4 ABLA: 3 PBLA: 5 vlPAG: 3

ACC, anterior cingulate cortex; PrL, prelimbic cortex; IL, infralimbic cortex. For other abbreviations, see list.

TABLE 2.

Surgical Coordinates for Unilateral Tracer Injections

Nucleus Targeted	Coordinates, from bregma (DV from skull surface)
ACC	AP = +1.6mm; DV = −3.5mm; ML = ±0.6mm
PrL	AP = +3.2mm; DV = −4.2mm; ML = ±0.8mm
IL	AP = +2.7mm; DV = −5.8mm; ML = ±0.8mm
NAcC	AP = +1.7mm; DV = −6.6mm; ML = ±1.6mm
NAcMs	AP = +1.7mm; DV = −7.5mm; ML = ±0.7mm
NAcLs	AP = +1.7mm; DV = −8.1mm; ML = ±2.0mm
ABLA	AP = −2.3mm; DV = −8.7mm; ML = ±4.8mm
PBLA	AP = −3.3mm; DV = −8.3mm; ML = ±4.8mm
VP	AP = −0.2mm; DV = −8.5mm; ML = ±2.4mm
vlPAG	AP = −7.8mm; DV = −6.0mm; ML = ±0.6mm

For all abbreviations, see list.

TABLE 3a.

Primary Antibodies Used for Immunocytochemistry

Antibody name	**Immunogen**	**Manufacturer, cat number, reference number, host**	**Dilution**
Anti-tyrosine hydroxylase antibody	Denatured tyrosine hydroxylase from rat pheochromocytoma (62kDa). UniProt Number: P04177.	EMD Millipore, Billerica, MA Cat# AB152, RRID:AB_390204 (Rabbit polyclonal IgG)	1:200
Anti-GAD67 antibody, clone 1G10.2	Recombinant GAD67 protein (67kDa). UniProt Number: Q99259	EMD Millipore, Billerica, MA Cat #MAB5406, RRID:AB_2278725 (Mouse monoclonal IgG2A)	1:200

TABLE 3b.

Secondary Antibodies Used for Immunocytochemistry

Conjugate and host	Against	Dilution	Supplier
Fluorescein (FITC) (Goat)	Anti-rabbit (H + L)	1:500	Jackson ImmunoResearch, West Grove, PA Cat# 111–095-003
Biotin (Goat)	Anti-mouse (H + L)	1:500	Vector Laboratories Cat# BA-9200
Fluorescein (FITC) - Avidin D		1:500	Vector Laboratories Cat# SP-2040